CONVECTIVE SCALE WEATHER ANALYSIS AND FORECASTING

James F.W. Purdom

Regional and Mesoscale Meteorology Branch/Development Laboratory
NOAA/NESDIS
and
Cooperative Institute for Research in the Atmosphere
Colorado State University
Fort Collins, Colorado

1. INTRODUCTION

The convective storm plays an important role across many scales in meteorology. For example, convective storms are important contributors to the total energy budget of the global circulation as well as summertime tropical regions through their release of latent heat, radiational properties, and convective cluster scale up moist/down dry vertical circulations they induce (Gray, 1973; Foltz and Gray, 1979). Locally, the convective storm lies at the heart of many weather-related events that affect everyday life. During the spring and summer months, tornadoes, flash floods, downbursts and severe thunderstorms pose serious threats to life and property throughout the United States. While the more notorious of such events receive Nation wide media coverage, the greatest weather-related killer in the United States is lightning from the everyday thunderstorm. That same "ordinary" thunderstorm can reek havoc in the construction industry while at the same time provide much needed water for agricultural purposes. In the above mentioned local areas, more precise very-short-range forecasting [often termed nowcasting (Browning, 1982)] is badly needed. Before accurate and precise local forecasting becomes a reality, an improvement in our understanding of convective storm genesis and development is required.

Understanding the forces that control the development and evolution of deep convection is one of the most important and challenging problems in meteorology today. It remains one of the most elusive problems to date even though various aspects of it have been vigorously investigated over the past quarter century. It is generally agreed that the development of a convective storm or storm array depends on the interaction of meteorological fields ranging from the synoptic scale cyclone down to the cloud condensation nuclei (Lilly, 1977). However, little is known about why a particular storm forms and develops the way it does, or why a convective array behaves in a particular manner. This is especially true for storms that form under weak synoptic scale forcing. Most of the available information about convective storm development and intensification is focused on either the large scale conditions favorable for convective development (Beebe and Bates, 1955; Miller, 1972), or the individual convective storm (Byers and Braham, 1949; Browning, 1964; Newton, 1963; Fankhauser, 1971, 1976; Brandes, 1978). As was pointed out a decade ago by Simpson and Dennis (1974), more is known about synoptic scale conditions favorable for convective development and cloud microphysics than is known about the mesoscale, which remains both poorly measured and poorly understood. That this problem still exists in 1984 can be readily verified - better understanding of mesoscale convective phenomena is one of the cornerstones in the planning of the National STORM Program (Zipser, 1984):

> "it is on the stormscale (or "mesoscale" to meteorologists) that the weather of greatest significance is actually experienced. It is mesoscale phenomena which must be understood ..."

That lack of information on the intermediate scale; the interaction between convective clouds and their mesoscale environment, has been mainly due to a gap in meteorological observing capability in the days prior to the high resolution geostationary satellite (Purdom, 1976).

Prior to satellites, meteorologists were forced to make inferences about the mesoscale from macroscale patterns. However, significant advances in that area have been made using data available from geostationary satellites. The sections that follow will show how satellite data can be used to improve our insight into the mesoscale behavior of the atmosphere. This in turn leads to a better understanding of the mesoscale process that lead to convective storm development.

2. APPLICABILITY OF SATELLITE DATA

2.1. Visible and infrared imagery

From the earliest days of meteorology, the importance of clouds in defining the state of the atmosphere has been recognized. As pointed out in the Handbook of Meteorology section on "Clouds and States of the Sky" (Schereschewsky, 1945):

> Clouds have been observed and used for short-period weather forecasting from time immemorial... Clouds are now considered essential and accurate tools for weather forecasting. Every feature of the air masses (discontinuity, subsidence, instability

and stability, etc.) is reflected by the shape, amount, and structure of the clouds. Thus close scrutiny of clouds will assist the analyst in identifying and analyzing air masses.

From its inception, the importance of cloud imagery to the meteorological satellite program has been recognized (Kellog, 1982). With the launch of TIROS-1 on April 1, 1960, cloud imagery from space became available. In the decades following the launch of TIROS-1, significant strides forward were made in synoptic scale weather interpretation. This was in large part due to the routine global cloud observations the satellite provided. As imagery from polar orbiting satellites helped advance our understanding of synoptic scale phenomena, imagery from geostationary satellites is helping advance our understanding of mesoscale phenomena. Why? Quite simply, prior to the geostationary satellite the mesoscale was a "data sparse" region, and meteorologists were forced to make inferences about mesoscale phenomena from macroscale observations. With GOES imagery, features that are infrequently detected at fixed observing sites are routinely observed.

With GOES data, a "reporting station" exists every 1 km using the information in visible data, and every 8 km with infrared data. The clouds and cloud patterns in a satellite image may be thought of as a visualization of mesoscale meteorological processes. When that imagery is viewed in animation, the movement, orientation and development of important mesoscale features can be observed, adding a new dimension to mesoscale reasoning. Furthermore, animation provides observations of convective behavior at temporal and spatial resolutions compatible with the scale of the mechanisms responsible for triggering deep and intense convective storms.

2.2. Sounding data

Satellite sounding data's applicability for use in mesoscale time frame applications is currently the subject of intense investigation. Considerable effort has been expended comparing individual satellite soundings with those from rawinsonde. For mesoscale applications, that might not be a meaningful approach to the problem. The two data sets are inherently different - each has its strengths and weaknesses. From rawinsondes we have 90 minutes of point observations (as the balloon rises) with high vertical resolution, poor spatial resolution, each 90 minute point observation set is taken by a different sensor, and sets of observations are taken at 12 hourly intervals (over the United States). Doswell and Lemon (1979) looked in detail at certain atmospheric parameter's importance in severe storm development. The major problem they encountered: the lack of resolution in the operational sounding data base (radiosonde spacing is approximately 400 km at 12 hr intervals) relative to the size of the phenomena being predicted. From GOES-VAS sounding data we have near instantaneous observations through a column in the atmosphere, moderate vertical resolution, high spatial resolution (in the absence of clouds), and one uniformly calibrated sensor making all of the measurements. With GOES-VAS, sounding data may be taken over an area the size of the United States at hourly intervals.

For many mesoscale applications, it is the gradient of atmospheric parameters and their changes in time that are important. This is one area where the new observational data from VAS, in combination with other data sources, should help lead to a better understanding of mesoscale atmospheric processes.

3. THE IMPORTANCE OF DIFFERENTIAL HEATING

An interesting observation concerning local trigger mechanisms for convective development is the strong influence exerted by differential heating. The land-sea breeze is a well understood differential heating phenomena that is routinely observed in satellite imagery. Another, that surely would have gone unnoticed without geostationary satellite imagery, is the effect of early morning cloud cover on afternoon thunderstorm development. Arc cloud lines, the driving force for deep convection over the southeast United States in summertime, represent another trigger mechanism due to differential heating - produced very quickly by rain-cooled air.

When using satellite imagery for mesoscale applications and applying image analysis concepts to phenomena such as those mentioned above, and to be addressed in the sections to follow, one must realize what they represent. That is, the setting up of local convergence zones that are generated due to differential heating. Other properties of the atmosphere help determine the effectiveness of those local mechanisms in their ability to generate new deep convection. They include instability, large scale dynamics, and the trajectory of the low level air with respect to the convergence zone (amount of time an air parcel will experience vertical motion in the local forcing region).

4. SEA, LAKE AND RIVER BREEZES

Although convective cloud development due to terrain influences may often be very complicated, when viewed with high-resolution visible GOES imagery, many of the cloud patterns are easier to understand. This is because the 1 km resolution of the imagery is close to the cumulus cloud scale, and the frequent interval between pictures allows one to observe convective development from its earliest stages through maturity.

The land-sea breeze, a consequence of differential heating between land and adjacent water, has been one of the most widely studied of any terrain phenomena (Haurwitz, 1947; Estoque, 1962; Pielke, 1973, 1974). Those authors point out a variety of factors that influence the development of the land-sea breeze. Among those factors are: 1) the shape of the coast line; 2) the direction and strength of the gradient wind; 3) friction; 4) the Coriolis effect; 5) the stability of the air mass; and 6) the land and water temperature difference. Items 4-6 will not be discussed here although one should realize the applicability of infrared data to item 6 and the potential of VAS sounding data to item 5.

Different curvatures in a coast line cause areas of convergence or divergence along the land-sea breeze front, thus leading to a local strengthening or weakening of cumulus activity along that front. As is pointed out by Pielke (1974), "Local maxima in vertical motion form in regions where the curvature of the coast line

accentuates the horizontal convergence created by the differential heating between land and water." Additionally, a small peninsula is generally an area of earlier strong convective development along the land-sea breeze front because the breezes formed along opposing shores merge near the peninsula's center. Figures 1, 2 and 3 are examples of early to mid-afternoon convection associated with the land-sea breeze regime over the Florida peninsula. Notice in those figures the enhanced convection along the land-sea breeze frontal zone as well as the pronounced clearing off shore. The effect of coast line curvature is most easily seen in the Gemini photograph (figure 1). In that figure notice the stronger convection in the Cape Canaveral peninsula region along Florida's east coast as well as the stronger inland penetration of the land-sea breeze's convection immediately south of the Cape. The effect of the gradient wind's flow on the land-sea breeze location is also apparent in figure 1. As one looks north from Cape Canaveral the land-sea breeze convection is observed to become continuously closer to the east coast. This is because the ridge of the Bermuda high lies east to west across central Florida and to its north the gradient wind strengthens in opposition to the inland penetration of the east coast land-sea breeze.

Convective development due to land and water interfaces also occurs regularly around lakes (Lyons, 1966). The factors influencing convective development are the same as those for the land-sea breeze. However, the low-level wind field becomes increasingly important the smaller the lake with which one is dealing. Figures 2, 3 and 4 all are good examples of lake effects on summertime convective development. Each also shows the effect of the gradient wind on the development of convection due to the lake breeze. In figure 2, a light low level southerly flow helps generate a small area of clearing downwind from Lake Okeechobee in south central Florida. Notice in figure 3 that a marked clearing extends westward from Lake Okeechobee: this is indicative of a strong low level easterly flow. Such downwind clearing from lakes, with enhanced convection bordering the clear region, is a common occurrence that is routinely observed with GOES imagery. Figure 4 shows the convective regime around the Great Lakes under a condition of north by northwesterly flow. Notice the lake breeze convection is close to the shore lines on the windward sides of the lakes and has a further inland penetration to their lee. One might envision frictional influences helping the inland penetration of the lake breeze convection along the eastern shore of Lake Michigan as well as the positioning of the convective line along the eastern shore of the Bruce peninsula which separates Lake Huron from Georgian Bay in southern Ontario.

While the effects of oceans, lakes and even cities (Changnon, 1976) on convective development have received considerable attention, relatively little work has been done concerning the effects of rivers and river basins on convective development. GOES imagery has shown that rivers and river basins at certain times exert a considerable influence on convective development. The influence has been most noticeable when the low-level winds were either nearly calm (generally less than 5 ms) or blowing parallel to the river basin. The effect of a river on convective

Fig. 1. Gemini photograph of Florida on 22 August 1965 at 1531 GMT.

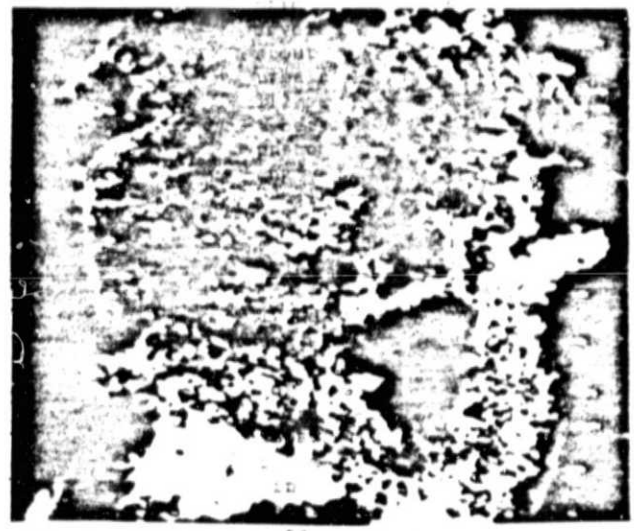

Fig. 2. GOES-East 1 km visible image, 25 June 1978 at 1730 GMT.

Fig. 3. GOES-East 1 km visible image, 21 July 1980 at 2130 GMT.

Fig. 4. Summertime DMSP photograph of convection around the Great Lakes.

development can be seen in figure 1, where the St. Johns river's influence on convective development can be seen as a meandering north to south line of clear skies in northeast Florida.

5. THE EFFECT OF EARLY MORNING CLOUD COVER

5.1. Weak synoptic forcing

Purdom and Gurka (1974) discussed the effects of early morning cloud cover on afternoon thunderstorm development under conditions of weak synoptic scale forcing. The situation was likened to that of the land-sea breeze, with the first showers forming in the clear region near the boundary of the early morning cloud cover - a sort of cloud-breeze front. Additionally, they found the slower heating rate in the early cloudy areas helped keep those regions free from convection for most of the day. Figure 5 is a good example of this phenomenon.

Fig. 5. GOES-East 1 km visible images, 27 May 1977 at 1530 and 1930 GMT. Convective development over Alabama due to early morning cloud cover. These images show the effect early cloud cover can have on afternoon thunderstorm development. Note that the early clear region in southwest Alabama becomes filled with strong convection during the day, while the early cloud region over the remainder of the state evolves into mostly clear skies. Also notice how the strongest activity later in the day develops in the "notch" of the clear region in south central Alabama, as one might expect from merging cloud breeze fronts.

While the effect of early cloud cover may most easily be thougnt of as a simple differential heating mechanism, for mesoscale applications our reasoning must extend beyond that point. Unlike the land sea breeze regime, the character of the cloud field is constantly changing: this can effect the development of instability since varying amounts of insolation will lead to differences in heating and mixing over the land area.

5.2. Strong synoptic forcing

Early morning cloud cover can also play an important role in helping set the stage for intense convection under conditions of strong synoptic scale forcing. Purdom and Weaver (1982) showed the importance of mesoscale boundary interactions in focusing tornado activity in the Red River Valley area on April 10, 1979. Figure 6 shows the location of one of the mesoscale frontal boundaries that helped focus that activity. The most probable cause of that meso-front was differential heating due to the cloudy (stratus) region to its east versus the clear area to its west. The mechanism which led to the development of the meso-front, and subsequent focusing of tornadic activity, also played an important role in the development of instability in the warm

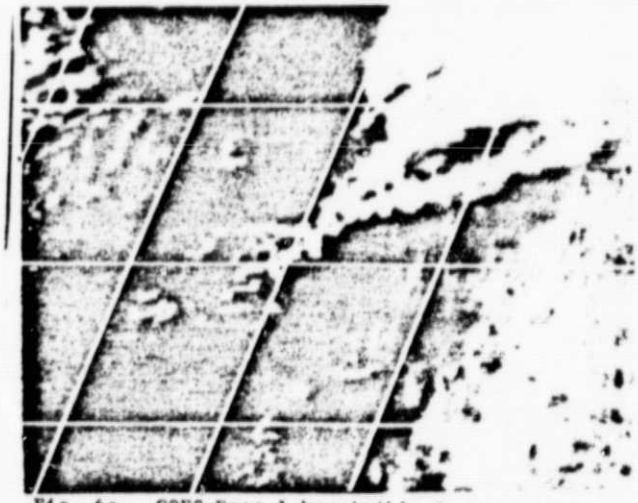

Fig. 6a. GOES-East 1 km visible image, 10 April 1979 at 2126 GMT.

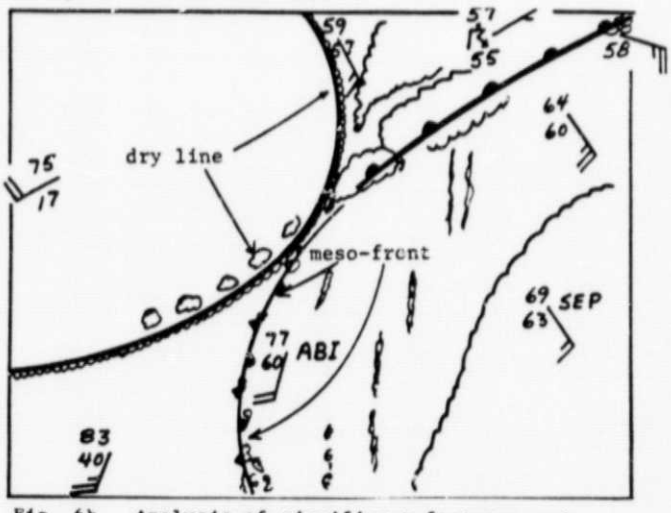

Fig. 6b. Analysis of significant features and cloud patterns from Fig. 6a.

sector. As the mesoscale frontal boundary moved eastward, mostly clear skies developed in the warm sector between the boundary and the stratiform overcast to its east. During that period Abilene (ABI) became clear while Stephenville (SEP) maintained its cloud cover. An analysis of surface static energy (Darkow, 1968) pointed to strong potential instability at both ABI and SEP (Purdom and Weaver, 1982). However, time series of horizontal cross sections from mesoscale rawinsonde data showed a marked decrease in the amount of negative buoyant energy at ABI and only a slight decrease at SEP: these changes are related to changes in cloud cover. Low level air, similar in character to that near ABI fed the tornadic storm system, allowing intense thunderstorms to develop.

Using a numerical boundary layer model, McNider and colleagues (McNider, et al, 1984) examined a case in which early cloud cover played an important role in the generation of a squall line when synoptic scale forcing was present. They found shading due to cloud cover to be fundamentally important in the formation of a local baroclinic zone and the development of low level convergence.

Thus we see that the effect of early morning cloud cover can be complicated indeed. It can act to set up a baroclinic zone (or reinforce an existing one) through differential heating. At the same time, it can effect the local destabilization of an airmass: a) if skies clear too quickly, moisture may be mixed to great depths making the region unsuitable for supporting strong moist convection; b) if the area remains cloudy, thunderstorms moving into the region might dissipate or weaken considerably due to the negatively buoyant low level air; c) if the area clears an hour or two prior to thunderstorms moving into it, sufficient heating and mixing at low levels may have occurred, priming the local air mass to support explosive convection. Use of VAS sounding channel data should aid in the assessment of the convective potential of such situations for mesoscale forecasting.

6. THUNDERSTORM OUTFLOW

6.1. Arc cloud lines

A number of works have addressed the thunderstorm and various phenomena associated with it. Among the earliest to address the outflow phenomena was Espy (1841). In his book The Philosophy of Storms, he spoke of the outflowing cool winds form storms at times being observed at a considerable distance from the storm. Later Humphreys (1914) pointed out the importance of evaporation of raindrops in the production of the storm's downdraft and subsequent cold outflow. Normand (1938) used thermodynamic diagrams to show the importance of both condensation and evaporation in allowing the thunderstorm system to gain kinetic energy from both its updraft and downdraft. It is important to note that in that paper he also pointed out the need for "work done by outside forces" to raise a parcel to a level where buoyancy forces alone could act to cause upward motion. While earlier works such as those mentioned above were important in laying a conceptual foundation for understanding the thunderstorm, the first in-depth study of that phenomena took place in Florida in 1946 and Ohio in 1947 with the Thunderstorm Project (Byers & Braham, 1949). In addressing outflow, they noted that the cold air outflow from a storm could cover an area larger than the storm, and that new cell development (with an aggregate of cells making up a thunderstorm) may occur in the vicinity of old cells whose outflows collide.

During the initial decade following the thunderstorm project, detailed analyses of mesoscale systems associated with thunderstorms showed a sharp pressure rise accompanying the systems arrival (Fujita, 1955, Fujita and Brown, 1958). Other phenomena noted with the passage of such systems were a wind shift that was often accompanied by an increase in wind speed, a temperature decrease, and in many instances rainfall. While it was generally recognized that evaporation of precipitation was an important factor in the production of the higher pressure and sharp pressure rise associated with such systems, it was Fujita (1959) who first quantitatively investigated that production. He showed that evaporation of raindrops in the downdraft was responsible for the development of a cold dome of air beneath the thunderstorm and the resultant mesoscale high pressure system. At the leading edge of this "mesohigh" was the thunderstorm gust front. Figures 7 and 8 from Fujita (1955 and 1959 respectively) relate two important points concerning this phenomena. Figure 7 illustrates the development of the mesoscale high pressure system and shows that the pressure surge line is at the leading edge of the mesohigh. Figure 8 illustrates the change in vertical temperature and moisture distribution within the cold dome produced by subsidence after the passage of the thunderstorm system. This subsidence of the cold dome is due to the cold dome's greater hydrostatic pressure, which causes it to sink and spread outward in an attempt to reach equilibrium with its surrounding environment.

It was Purdom (1973) who first pointed out that in satellite imagery, the leading edge of the meso-high appears as an arc-shaped line of convective clouds moving out from a dissipating thunderstorm area. The arc-shaped cloud line is

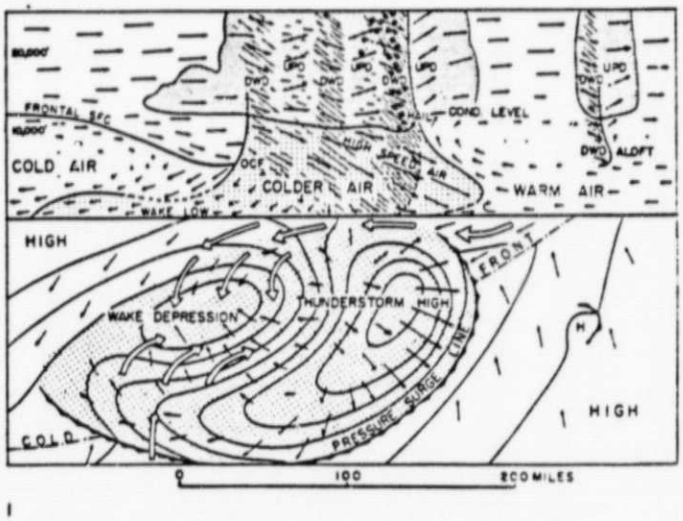

Fig. 7. From Fujita 1955 illustrating the importance of rain-cooled air in the production of the mesoscale high pressure system.

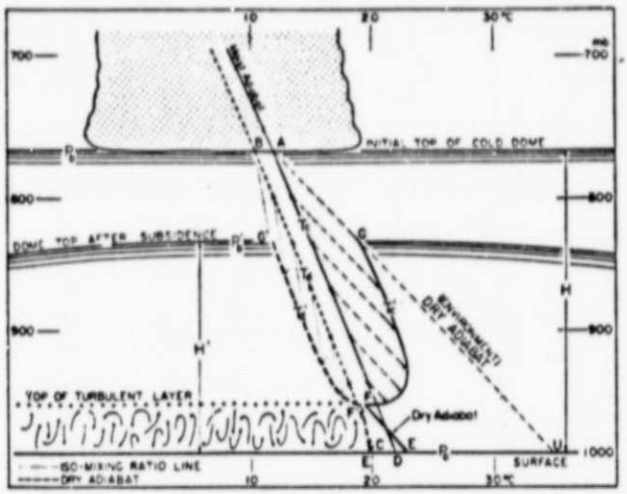

Fig. 8. From Fujita 1959 illustrating the importance of subsidence within the cold dome, after the passage of the thunderstorm system, which leads to clearing in that region.

Fig. 9. Photograph taken from a manned spacecraft of thunderstorm activity and resultant clearing within the cold dome.

normally composed of cumulus, cumulus congestus, or cumulonimbus clouds. Later Purdom (1979) was to introduce the concept of "convective scale interaction" due to arc cloud lines and discuss its role in controlling the development and evolution of deep convection. This is discussed further in the next section.

Figure 9 is a photograph of an arc cloud line taken from a manned spacecraft. Note the large circular clear region: this would be due to subsidence within the cold dome. Figure 10 shows the characteristic appearance of arc cloud lines in satellite imagery. Figure 11, is a mesoscale analysis/nephanalysis in which the arc cloud lines in Figure 10 were analyzed with the aid of 15 minute interval satellite images. In this case, interaction between the arc cloud and frontal boundary in Oklahoma produced a large

Fig. 10. GOES-East 1 km visible image, 26 May 1975 at 2000 GMT.

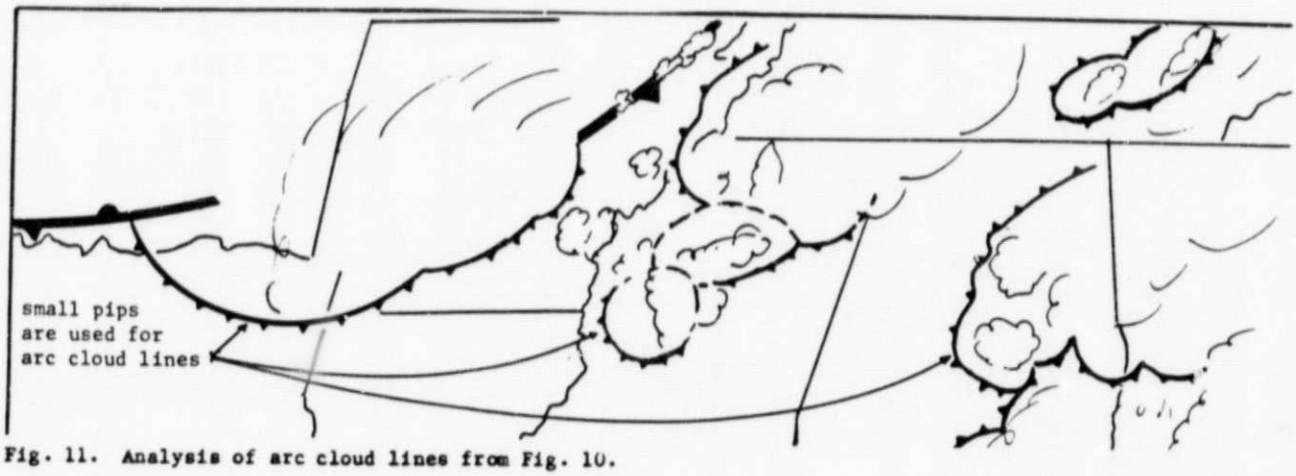

Fig. 11. Analysis of arc cloud lines from Fig. 10.

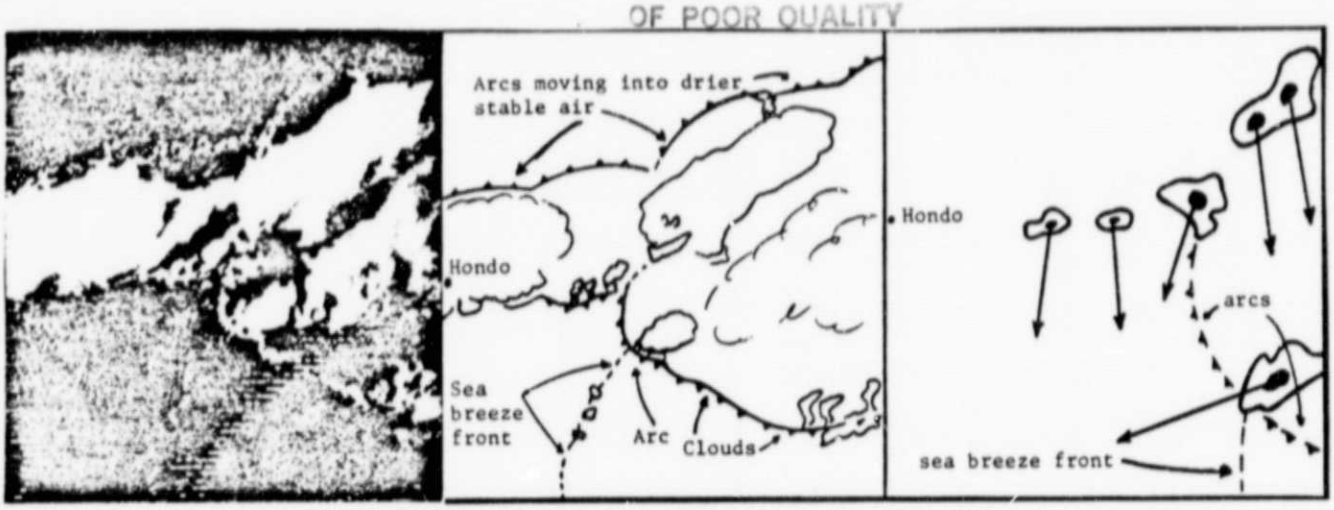

Fig. 12. Three panel figure showing GOES-East visible image for 1520 CST, 30 July 1980 (left), an analysis of the image (middle) and radar echo movements centered on 1600 CST (right). The large thunderstorm generated at the sea breeze and arc cloud line merger propagated (continuously regenerated) along the moving intersection of those two boundaries.

severe thunderstorm (see Purdom, 1983). Figure 12 is another example of an arc cloud line as detected in GOES imagery. In this case interaction of an arc cloud and sea breeze front in Texas produced a large thunderstorm (Zehr, 1982). The thunderstorm generated at that intersection moved to the west, while other thunderstorms in the area moved to the south. Two important points to consider when examining these figures are: 1) the "anomalous" movement of the echo at the sea breeze/arc cloud junction - this can be explained by continuous regeneration along that moving intersection; and 2) the arc cloud lines shown in the satellite image were not detected by radar.

6.2. Convective scale interaction

NESDIS and NASA, recognizing the importance of geostationary satellite data in understanding convective development, have operated the GOES system in a special rapid interval (3 to 5 minute) imaging mode on selected days during convective seasons since 1975. Those unique data sets have allowed observations of convective behavior at temporal and spatial resolutions compatible with the scale of the physical mechanisms responsible for triggering deep and intense convective storms. Movie film strip analyses of those data show that convective scale interaction is of primary importance in determining the development and evolution of deep convection (Bohan, 1981). This interaction manifests itself as the merger and intersection of thunderstorm-produced arc cloud lines with other convective lines, areas and boundaries (Purdom, 1979). Pertinent conclusions can be summarized as follows:

1. Thunderstorm-produced outflow boundaries (arc clouds) are of primary importance in the formation and maintenance of strong convection;
2. Outflow boundaries may maintain their identity as arc clouds for several hours after the convective array that produced them has dissipated;
3. Deep convective development along an arc cloud line is a selective process - highly favored where two arcs intersect or where an arc moves into a convectively unstable region; and
4. In a weakly forced atmosphere, arc boundary interactions determine the location of the majority of new thunderstorms by the end of the day.

The convective scale interaction process is fundamental in the evolution and maintenance of deep convective activity--until recently, it was only observed by satellite. In fact, thunderstorm evolution that appears as a random process using conventional radar is often observed to be well ordered when viewed in time lapse using satellite imagery.

Since this earlier work of Purdom numerous investigators have begun to study the effects of outflow on new storm generation. Achtemeier (1983) in studying the relationship between the surface wind field and convective precipitation in Missouri found,

> the preferred area for new cell development were in agreement with the findings of Purdom ... eight of the fourteen rain cells related to gust fronts formed at the intersection of gust fronts, or at the intersection of gust fronts with network scale convergence zones.

Holle and Maier (1980) traced two outflows across the FACE mesonetwork and found an intense thunderstorm with a weak tornado formed at their intersection. Droegemeier and Wilhelmson (1983) are currently using the 3D cloud model to study the convective scale interaction phenomena. Figure 13 is an adaptation from Droegemeier and Wilhelmson (1983), and shows their results using a three dimensional numerical cloud model to study thunderstorm outflow collision with a convective cloud line. In that simulation they found a deep convective cloud with maximum vertical motions on the order of 19 ms^{-1} developed where the outflow interacted with the convective cloud line. They noted that such convective scale interaction was not observed in the simulation where the outflow moved into clear regions. Convective scale interaction has also recently been observed by Wilson (1984) using Doppler radar data to investigate new thunderstorm generation at the collision of two thunderstorm outflows.

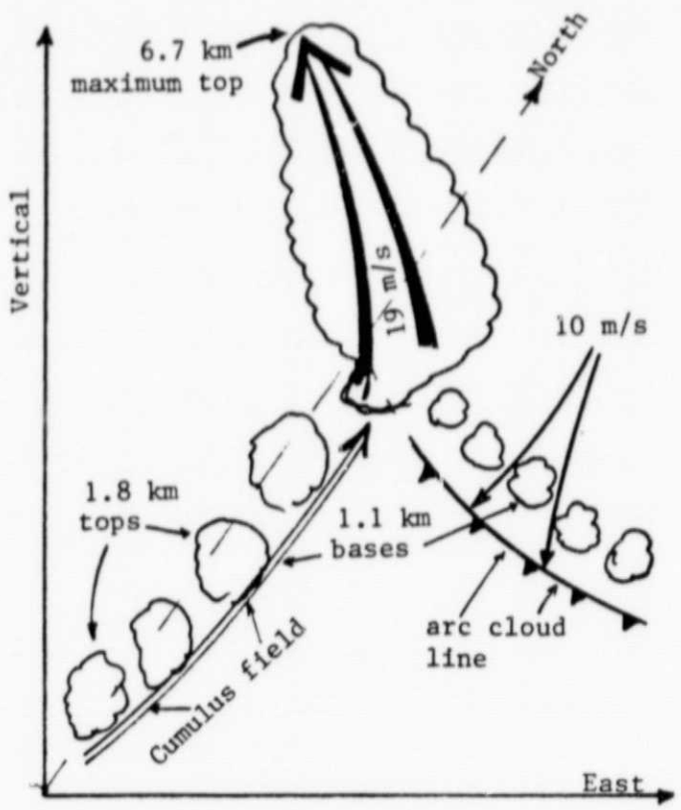

Fig. 13. Adaptation of numerical modelling results of thunderstorm outflow collision with a convective cloud line, from Droegemeier and Wilhelmson.

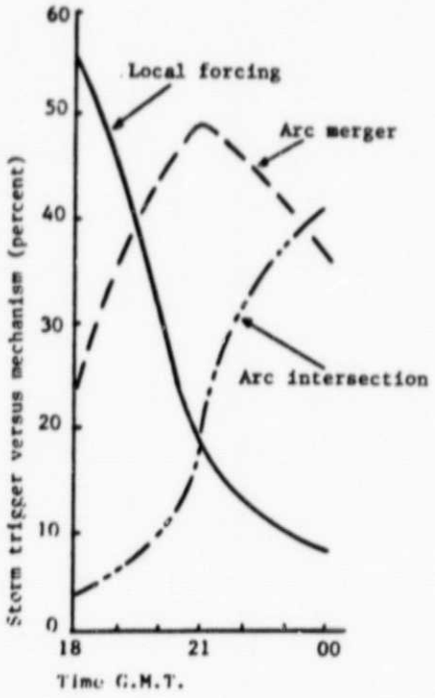

Fig. 14. Distribution of convective generation mechanisms due to arc cloudlines (merger and intersection) and other mechanisms (local forcing).

6.3. Convective rainfall under weak synoptic scale forcing

Using GOES satellite imagery, Purdom and Marcus (1982) classified convective development over the southeast United States. Their results, Figure 14, show that when the most intense convection has developed, the dominant generation mechanism is convective scale interaction. The results of Purdom and Marcus have been extended to include rainfall over the southeast during the study period. Figure 15 shows the cumulative amount of rainfall (normalized) by hour for all hourly rainfall recording stations in the study area: notice the dominance of arc generated rainfall. During the study period no mesoscale convective complexes (Maddox, 1980) moved through the study area.

6.4. The structure of arc cloud lines

The character of arc cloud lines has been the subject of direct aircraft measurements (Sinclair & Purdom, 1982, 1984). The purpose of those flights was to gain knowledge concerning the dynamic and thermodynamic characteristics of arc cloud lines as they relate to future convective development (including tornadic storm formation). Flights were made in the subcloud layer above the density surge line, DSL (Sinclair & Purdom, 1982), as well as through the DSL (Sinclair & Purdom, 1984). Results from the aircraft observations,

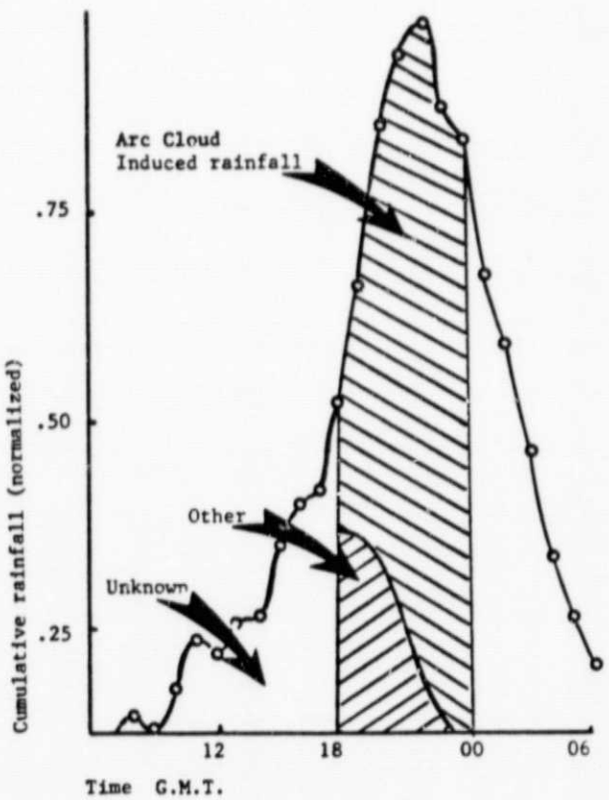

Fig. 15. Rainfall distributed by mechanism for the study period in Fig. 14.

shown schematically in Figure 16, point to the importance of arc cloud lines in the production of both vorticity and convergence. Furthermore, it was found that the lateral extent of the vertical motion field along the arc compared to that of the cloud scale indicates that the main driving force for initial cloud development along the arc line is controlled by thunderstorm outflow(s) interacting with the convectively unstable air of the environment. The individual cumulus cloud scale motions along the arc line can then be visualized as being superimposed on this somewhat larger scale, initiating process.

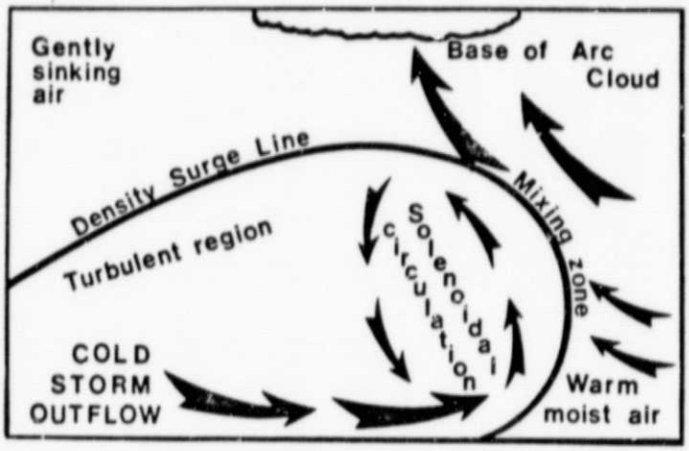

Fig. 16. Schematic illustration of arc cloud line features as derived from aircraft penetrations.

Arc cloud lines and their associated DSL region can pose extreme hazards to aircraft operations. One of several critical situations might involve an arc cloud line approaching the end of an airport runway with its parent thunderstorm 15 to 20 km away. An aircraft in a landing pattern might circumnavigate the thunderstorm and then descend through the top of the DSL. If the outflow is strong, a tailwind of 20 to 30 m/s or greater might suddenly be encountered. Depending on aircraft speed prior to its descent, the loss of relative flow across the wing in the DSL might cause critical sink rates which could lead to an aircraft accident. One should be aware that arc cloud line interactions were in part responsible for the aircraft accident that claimed 153 lives in New Orleans, Louisiana on July 9, 1982 (Caracena, et al, 1983).

7. MESOSCALE CONVECTIVE SYSTEMS

7.1. Squall line development

Generally, organized convergence lines that trigger strong convection (such as fronts, dry lines or pre-frontal convective lines) are detectable in satellite imagery prior to deep convective development along them (Purdom, 1976). An example of a frontal system that develops into a severe squall line is shown in Figure 17. Early squall line developments of this type are routinely detected in GOES imagery prior to deep convective development on them and their being detected by radar. In this case a Pacific front which extended from eastern South Dakota and Nebraska into central Kansas developed into a line of severe thunderstorms as it moved into Minnesota and Iowa later in the day. Near the time of the latest image shown in Figure 17, large hail and funnel clouds were reported in South Dakota, a tornado injured six people in Minnesota, and a weak tornado was reported in Iowa. Later in the evening, six people were injured and one was killed by tornado activity in Minnesota, severe winds were reported in Iowa, and the thunderstorms in central Kansas had numerous funnel reports, one confirmed tornado and several reports of hail.

7.2. Mesoscale convective complexes

While squall lines generally form under conditions of moderate to strong synoptic scale forcing, a different type of highly organized mesoscale convective system which forms under conditions of weak synoptic scale forcing has been recently documented by Maddox (1980). This important class of spring and summertime convective weather system, which occurs most often over the central United States during the late evening and nighttime hours has been given the name Mesoscale Convective Complex (MCC). The MCC's appear to be a convectively driven weather system - their dynamics are not well understood although they appear to have many characteristics similar to those of tropical convective systems. MCC's have been observed to interact with and modify the larger scale environment in which they are embedded. By influencing the larger scale environment they affect downstream weather long after their demise.

As with arc cloud lines, MCC's were not recognized prior to observations afforded by GOES. Table 1, from Maddox (1980) describes the physical characteristics of an MCC based on satellite infrared imagery analysis. Figure 18 shows the characteristic appearance of an MCC in satellite

Table 1. Mesoscale Convective Complex (MCC) (based upon analyses of enhanced IR satellite imagery)

Physical characteristics	
Size:	A - Cloud shield with continuously low IR temperature $\leq$ -32 C must have an area > 100,000 km B - Interior cold cloud region with temperature $\leq$ -52 C must have an area > 50,000 km
Initiate:	Size definitions A and B are first satisfied
Duration:	Size definitions A and B must be met for a period > 6 h
Maximum extent:	Contiguous cold cloud shield (IR temperature $\leq$ -32 C) reaches maximum size
Shape:	Eccentricity (minor axis/major axis) > 0.7 at time of maximum extent
Terminate:	Size definitions A and B no longer satisfied

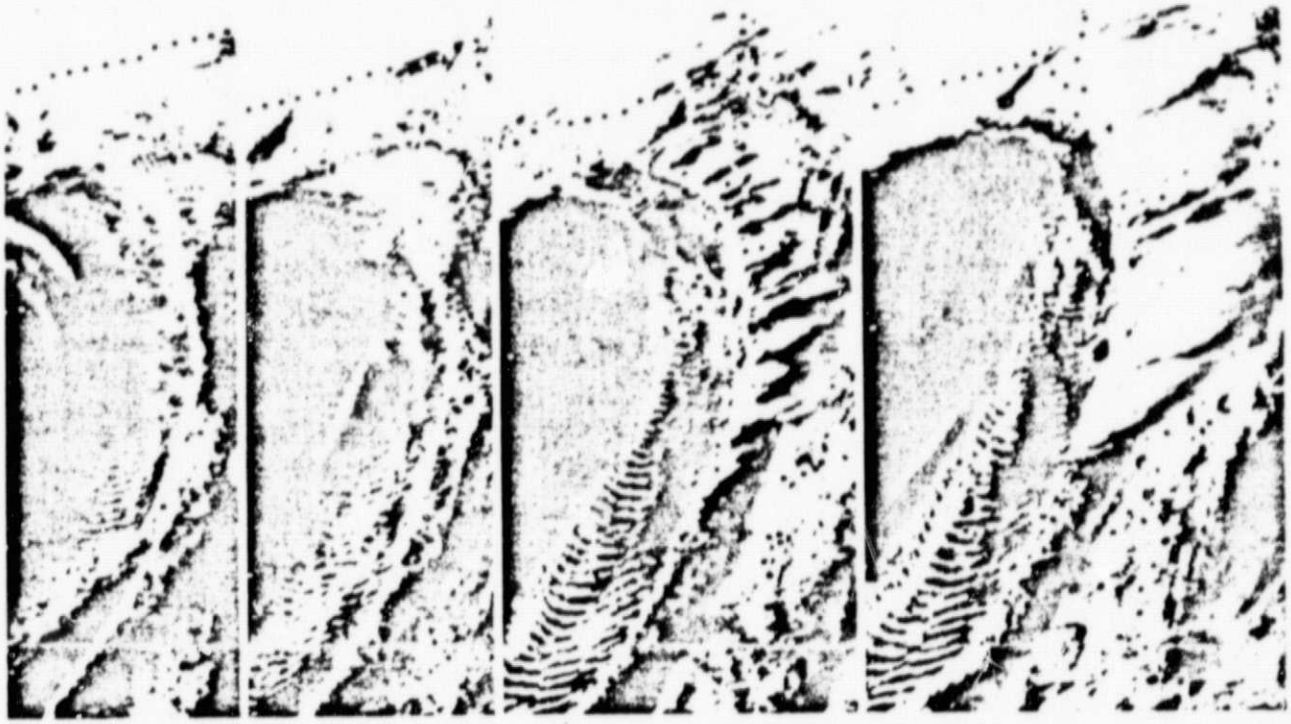

Fig. 17. GOES-East 1 km visible images, 14 June 1976 at 1900 GMT, 2000 GMT, 2200 GMT and 2300 GMT; a typical example of squall line development.

imagery. It should be noted that MCC's produce much of the beneficial rainfall that occurs over the central plains of the U.S. However, they are also noted to be prolific producers of severe weather. In fact, Maddox (1980) shows that for the 43 MCC's that occurred in the 1978 convective season there were 17 cases with flooding and/or heavy rain, 17 cases with tornadoes, 21 cases with severe wind, 22 cases with hail - only 8 of the 43 cases had no severe weather reported. Twenty five deaths and over 135 injuries were attributed to the weather associated with 9 of the severe MCC's.

Fig. 18. GOES-East enhanced infrared image of a typical mesoscale convective complex over the central United States on 22 June 1981 at 1500 GMT.

8. ISOLATION OF SEVERE CONVECTIVE STORMS USING VISIBLE IMAGERY

8.1. Squall line boundary interaction

As shown in the previous section, organized convergence lines that trigger strong convection (dry lines, fronts, etc.) are detectable in GOES imagery prior to deep convection forming on them. Under proper dynamic forcing when the thunderstorms that form along such lines interact with other boundaries severe storms develop (Miller, 1972). For example, on May 6, 1975, strong tornado activity that began in northeast Nebraska developed southeastward into the Omaha area along a squall line and warm frontal intersection. Figure 19 shows how these features as identified in satellite imagery could be tracked during the outbreak. The developing squall line appeared as an organized line of convective clouds along a surface windshift line separating moist and dry air. The warm frontal boundary appeared as another organized line of convection separating warm moist air embedded in southerly flow from slightly cooler and drier air in southeasterly to easterly flow. Other clues helpful in the precise location of the warm frontal boundary may be found by inspecting the change in cloud type across it (cumulus versus stratus), as well as through cloud track winds.

8.2. The importance of prior convective activity in severe storm development

Arc clouds and their convective scale interactions are a natural part of the convective cloud genesis and evolution process. They occur anywhere and, because of the strong vorticity and convergence that they produce, are often associated with severe thunderstorm development. An extreme example was the severe storm associated

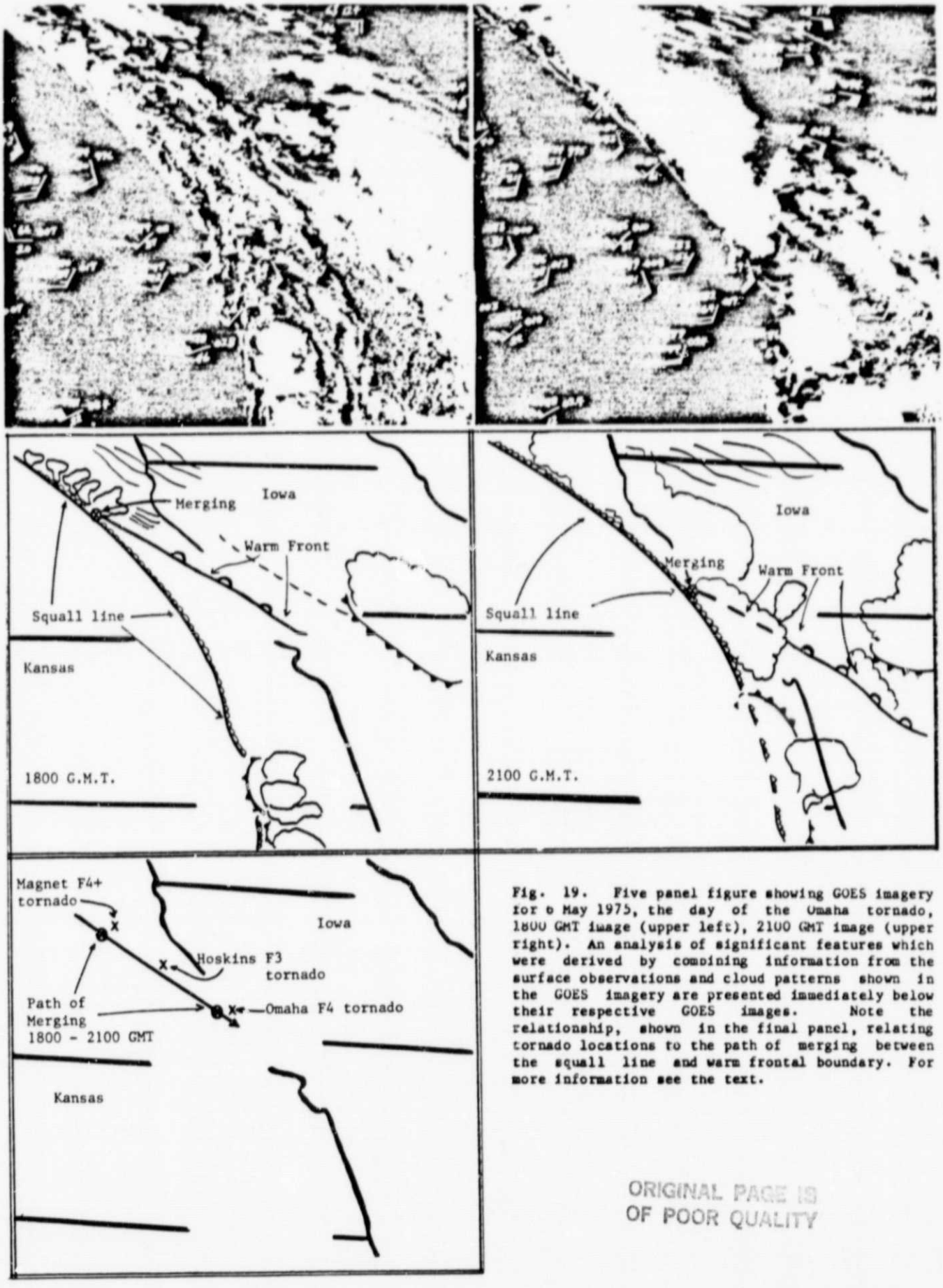

Fig. 19. Five panel figure showing GOES imagery for 6 May 1975, the day of the Omaha tornado, 1800 GMT image (upper left), 2100 GMT image (upper right). An analysis of significant features which were derived by combining information from the surface observations and cloud patterns shown in the GOES imagery are presented immediately below their respective GOES images. Note the relationship, shown in the final panel, relating tornado locations to the path of merging between the squall line and warm frontal boundary. For more information see the text.

with the most destructive tornado in Wyoming history (Parker & Hickey, 1980). Figure 20 is a satellite view of the mesoscale convective environment prior to the Chicago tornadoes of June 13, 1976. Tornadic activity began shortly after the west to east oriented arc cloud line south of Lake Michigan moved north and interacted with the storm over the Chicago area! Recent modeling efforts (Klemp & Kotunno, 1983) support these observations from satellite imagery on the importance of arc cloud lines (outflow) in producing tornadoes:

> We emphasize that within the simulation, large positive vorticity does not first develop at midlevels and then descend within the storm to the ground; rather, strong vertical vorticity is generated at low levels in response to the increased convergence.

Arc cloud lines are not the only satellite indicator of previous convection. Figure 21 is a good example of how satellite imagery may be used to identify a transition zone between an unstable airmass and a more stable mesoscale airmass generated by earlier thunderstorm activity. In that figure, note the cumulus cloudiness at A and the wave cloud dominated air at B. Both are low-level cloud features. In this particular case the wave dominated air had been stabilized by early morning thunderstorms in the area. The low-level air mass boundary that existed between these waves and cumulus streets was instrumental in the development of tornadic storms upon interaction with a cold frontal zone.

The importance of prior convection in setting the stage for tornadic storm activity was vividly demonstrated by a storm system that moved through the southeastern United States on March 28, 1984 (Purdom, 1984). Thunderstorm activity that had moved through the area during the early morning hours produced a well-defined outflow boundary which extended westward from South Carolina across Georgia and into Alabama. This boundary moved slowly northeastward during the day, and by 3:30 PM EST, was evident in satellite imagery as a line of organized cumulus congestus clouds extending across South Carolina into North Carolina, Figure 22. The large storm in northeast Georgia lies at the junction of the convergence boundary and a subsynoptic low. That storm developed into a large super cell which tracked east-northeast along the boundary producing most of the intense killer tornado activity, Figure 23 (see also Figure 25).

It is interesting to note that for both March 27th and 28th strong synoptic scale forcing set the stage for severe storm development. However, the major meteorological difference between the 28th, (a long track tornadic super cell producing killer tornadoes) and the 27th (numerous reports of severe activity but no major tornadoes) was the existence of a well organized low level convergence boundary and mesolow to help support the super cell's growth and development.

8.3. Vertical wind shear

It is well known that vertical wind shear plays an important role in determining the character of storms that evolve in a mesoscale environment (Newton, 1963). Furthermore, recent numerical cloud modeling studies have shown the importance of vertical wind shear in the formation

Fig. 20a. GOES-East 1 km visible image, 13 June 1976 at 2245 GMT.

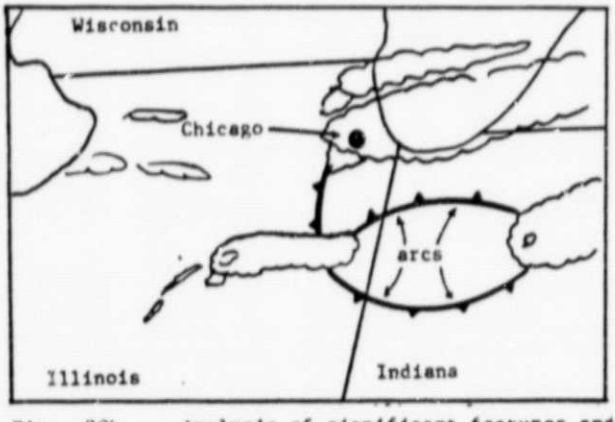

Fig. 20b. Analysis of significant features and cloud patterns from Fig. 20a.

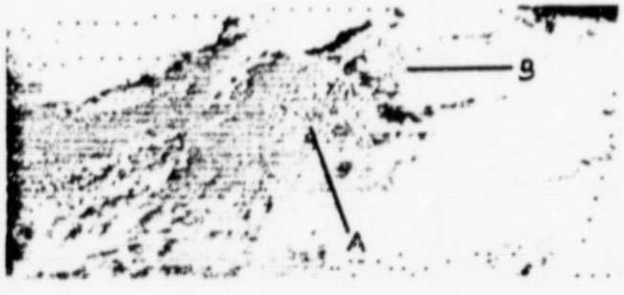

Fig. 21a. GOES-East 1 km visible image, 2 May 1979 at 2030 GMT.

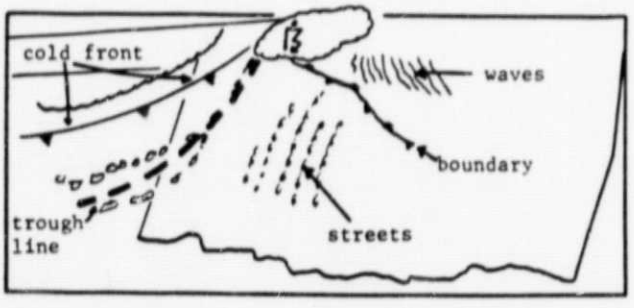

Fig. 21b. Analysis of significant features and cloud patterns from Fig. 21a.

Fig. 22a. GOES-East 1 km visible image, 26 March 1984 at 2030 GMT: note the boundary.

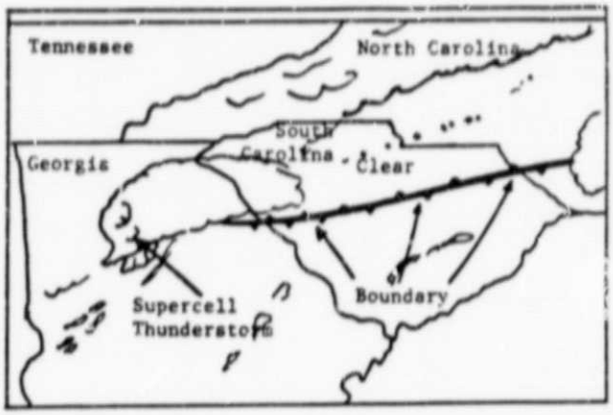

Fig. 22b. Analysis of significant features and cloud patterns from Fig. 22a.

of rotation in growing thunderstorms (Klemp and Wilhelmson, 1978; Bleckman, 1981). However, a severe storm environment is one in which both the dynamic and thermodynamic characteristics of the atmosphere are changing on mesoscale space and time domains. Determination of vertical wind shear in regions of growing cumulus clouds using rapid scan satellite imagery is a feasible method of studying mesoscale variations in that parameter over large areas.

After thunderstorms have developed, animation of the imagery may be done relative to the thunderstorm. In such cases, the flows at different levels with respect to the storm may be inspected. Such a study was undertaken for the storm which produced the Wichita Falls tornado on April 10, 1979 (Purdom, et al, 1984). A GOES-East view of the storm at 0:15 PM CST is shown in Figure 24 along with the relative flow derived from 3 minute interval GOES-East data at low, middle and high levels with respect to the Wichita Falls storm. Figure 25, similar to figure 24, shows the storm relative flow for the 28 March 1984 super cell storm discussed in the previous section. It is interesting to note how closely those relative flows compare to that proposed by Browning (1964) for severe storms which travel to the right of the wind, and storm relative proximity soundings (Maddox, 1976). Being able to diagnose storm relative flow has important implications for defining mesoscale regions that are favorable for the production of rotating storms and severe weather.

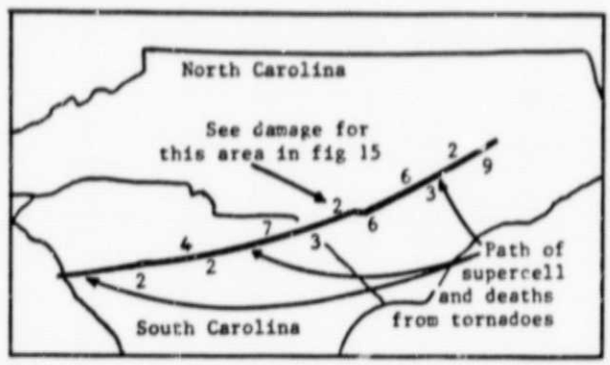

Fig. 23. Paths of super cell which produced significant tornadoes, and deaths associated with those tornadoes for 28 March 1984.

8.4. Overshooting tops

Overshooting thunderstorm tops as detected in satellite visible imagery, and how they relate to severe weather, continues to be an area of active investigation. Early work in this area was done by Pearl (1974) and Fujita, et al, (1976) in which photographs of overshooting tops taken from Lear Jets were correlated with overshooting tops as detected in satellite imagery and severe weather. Pearl's study used ATS data, while Fujita's study

Fig. 24a. GOES-East 1 km visible image, 11 April 1979 at 0015 GMT.

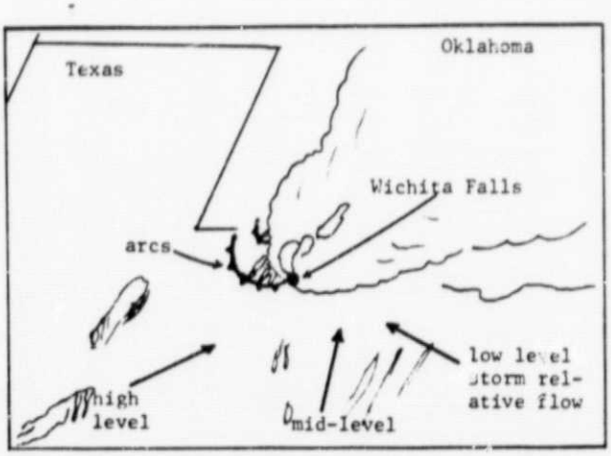

Fig. 24b. Analysis of cloud relative flow and significant features for the image in Fig. 24a.

used the higher resolution data available from SMS (GOES). Hassler (1981) has found similar results, correlating severe events with overshooting tops, using stereo measurements of cloud top characteristics obtained by combining GOES-East and GOES-West data.

Overshooting tops are generally associated with updraft regions that penetrate well above the equilibrium level as defined by the top portion of the spreading thunderstorm anvil. While overshooting tops are often associated with intense convection, there is one serious limitation in using them as storm intensity indicators: they are only detectable for a few hours in the early morning or late afternoon when the sun is low enough on the horizon for the tops to cast shadows on the underlying anvil.

9. INFRARED IMAGERY

9.1. Enhancing infrared imagery

As subjective interpretation of remotely sensed data takes on increasing importance in nowcasting, the question of how to present that data for use by a forecaster becomes significant. Data from a single sensor or combination of sensors must be presented so that important features are readily detectable, while at the same time leaving other features in a resolvable form. GOES infrared data provides information of rather coarse spatial resolution, high thermal resolution, and of a temporal resolution that may range from 3 minute intervals to the normal 30 minute intervals. When GOES infrared data are expanded for display over areas comparable to those covered by a 1 km visible resolution image, or the area covered by a radar, they appear blocky (Figure 26). Depending on the type thermal enhancement curve that is used, the data may appear as discontinuous, with several degrees of a temperature range lumped into the same gray shade, as in Figure 26. Both blockiness and improper enhancement detract from using the GOES infrared data for mesoscale applications. In such images, the regular-shaped rectangles and poor enhancement may actually draw attention away from the information in the image. This is true for both single picture mesoanalysis and for viewing the imagery in animation. With those thoughts in mind Purdom and Vonder Haar (1983) developed a product to (1) deblock the data while improving its spatial resolution, and (2) present temperature values in a continuous, easily discernible form through selective color enhancement of the infrared data. The deblocking of the infrared data effectively contours the imagery at 1.0 C intervals. When color enhancement is used with the deblocked image, the resultant image (final product) appears with distinct, but continuous, 1.0 C interval shades of color. Examples of the final product are shown in Figures 27 (same storm as Figure 26), 28, and 32. Note in those figures that the improved infrared image appears as one might expect a cloud features to appear, smooth and continuous - not blocky.

9.2. Combining infrared imagery and radar data

For almost the past forty years, radar reflectivity has been the norm for remotely assessing a thunderstorm's intensity, while GOES infrared data's use in that area has yet to span a decade. How do the two data sets relate in the area of storm intensity assessment? Both satellite and radar data have important roles to play in that area. Satellite data provide information on cloud top mean vertical growth rates, cloud top temperature and anvil expansion rates to help assess storm intensity, while conventional radar data provide information about reflectivity and volumetric echo properties and their changes in time.

The utility of satellite and radar data in thunderstorm analysis has been the subject of limited investigation. Negri and Adler (1981) found that the location of satellite defined thunderstorms coincided with radar echo locations and that radar reflectivity correlated with satellite based estimates of intensity. Similar results were found concerning satellite defined thunderstorm tops and those defined by radar by Purdom, Green and Parker (1982), and Green and Parker (1983).

The question of how to present the two products to a user for mesoscale applications continues to be an interesting area for investigation. Reynolds and Smith (1979) demonstrated the concept of a composite radar and satellite display to study severe storm development and convective rainfall. Green and Parker (1983) used the improved product described in the previous section to develop a composite satellite infrared/doppler radar image for the purpose of evaluating radar echo changes in time as they relate to infrared cloud top behavior. That such an effort is not a trivial problem can be seen by inspection of figure 27. Notice how the strong echo return at upper levels for the 164 KHI scan matches the infrared cold top region, while for the 158 KHI scan it does not. This is mainly because of the vertical structure of the radar echo. Since vertical wind shear varies considerably from one type meteorological thunderstorm regime to another, that information should be taken into account when satellite and radar data are combined. Furthermore it is better to combine information concerning the vertical structure of the radar echo with cloud top information than to use radar information from only a single level.

Figure 28, is a 1 and 15 km radar CAPPI scan (green and brown) mapped as a transparency on a satellite infrared cloud top temperature field. Notice how the 1 C isotherm contours can be followed through the echo. This case has been studied using 3 minute interval improved GOES infrared data and 4 minute interval CAPPI scan data at elevations from 1 km to 17 km (Fujita, 1982; Green & Parker, 1983). Among the interesting findings from those studies were:

1) When storms are forming in a line, with one storm downwind from another, the downwind storms cloud top temperature may appear warmer than it should due to wake cirrus masking. Furthermore, to be able to accurately follow the evolution of these tops and to observe this masking requires satellite imagery at a frequency near 3 minutes.

2) The coldest satellite cloud top temperature in an anvil may not necessarily overlie the low level core of highest radar reflectivity. There may be information in this offset concerning storm severity.

Fig. 33. GOES-East 6.7 μ water vapor image and storm relative flow, 28 March 1984 at 2345 GMT. (out of sequence)

Fig. 25. GOES-East 1 km visible image, 28 March 1984 at 2145 GMT showing storm relative flow at low (L), mid (M) and high (H) levels as well as -46 C isotherm divergence within anvil.

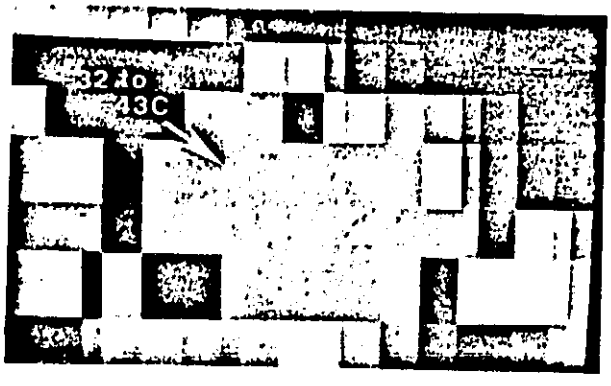

Fig. 26a. Normal GOES-IR image with common black and white temperature enhancement (curve Mb).

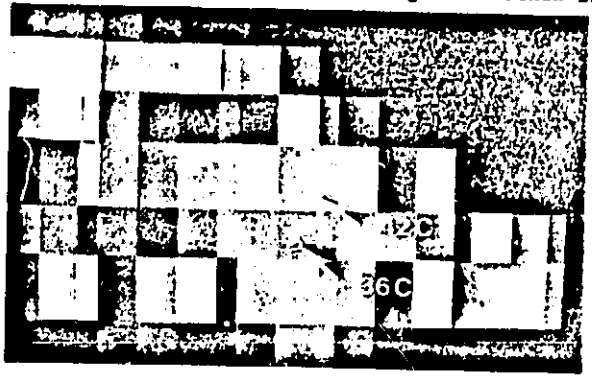

Fig. 26b. Storm in Fig. 26a, but with color temperature enhancement.

Fig. 27a. Improved infrared product with 1 C isotherm contours for storm in Fig. 26.

Fig. 27b. RHI scan at 158 for storm in Fig. 27a.

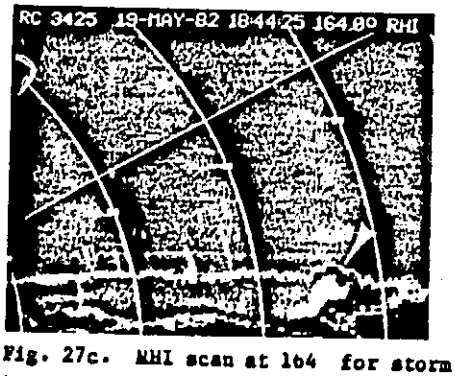

Fig. 27c. RHI scan at 164 for storm in Fig. 27a.

Fig. 28. Satellite and radar composite for 2303 GMT, 2 May 1979, (1 km and 15 km CAPPI).

3) In measuring cloud top growth characteristics using satellite infrared data, one must be aware that cirrus masking may make results less accurate for certain storms. Furthermore, one can use CAPPI displays to help insure that the correct infrared anvil area is being matched with the correct echo.

4) The horseshoe cold ridge, or "V notch" observed in satellite infrared imagery is an indicator of intense local convection. Storms whose anvils exhibit that characteristic should be closely monitored for severe weather.

At the time of the image in Figure 28, echoes A and B had merged at low levels while echo C was developing rapidly. The Lahoma tornado (F4 intensity) had just ended in echo A and the Waukomis downburst was about to begin, while the Orienta tornado (F4 intensity) was about to dissipate in echo A.

9.3. Clues in infrared imagery for severe storm identification

Since the earliest days of geostationary meteorological satellites, measurements of a variety of cloud top properties have been made in attempts to diagnose storm severity. Using ATS imagery, Sikdar, et al, (1970) and Purdom (1971) related thunderstorm anvil growth rates to the occurrence of severe weather. Those results showed promise; however, further developments awaited the arrival of GOES and its more quantifiable infrared data. Using GOES infrared rapid scan data, Adler and Fenn (1977, 1979) correlated the areal expansion rate of isotherms colder than the tropopause for severe storm occurrence. Figure 29, from Adler and Fenn (1977), indicates the rapidly growing nature of a severe storm at Miles City, MT that produced winds of over 80 knots and 2-inch hail. Along a similar vein, Pryor (1978) performed a detailed study using rapid scan GOES infrared data to compare severe events with cloud top temperatures which were colder than the environmental tropopause temperature. In that study, Pryor found only those thunderstorms with GOES infrared cloud top temperatures colder than the tropopause produced severe weather. In a similar study, Reynolds (1979) found a positive relationship between the occurrence of hail and infrared tops colder than the tropopause.

Fujita (1978) discussed characteristics of anvil tops of severe storms based on the pattern of equivalent black body temperature as shown in enhanced GOES infrared imagery. The signature appears as a cold "V" shape in the anvil top, with marked downstream warming from the center of the "V". Figure 30, from Fujita, (1981), shows a detailed analysis of GOES infrared data for the storm that produced the Grand Island, NB tornadoes - note the cold "V" ("horseshoe ridge"), the intense overshooting cold tops, and the downstream warm region ("wake"). This type anvil signature has also been documented by Reynolds (1979) for severe hail storms. Using operational GOES data, McCann (1981) has shown a good correspondence between the enhanced "V" notch signature and severe weather.

Weaver and Purdom (1983) performed an extensive case study analysis of an intense tornadic storm outbreak using 5 minute interval GOES visible and enhanced infrared imagery. Figures 31 and 32 are from that study. Inspection of the visible imagery (figure 31) reveals two overshooting tops in the thunderstorm complex in southwestern Oklahoma. Also note that in the infrared data (figure 32), the regions identified as overshooting tops each has an associated cold top. At this image time the minimum temperature observed (same for both tops) was -69 C, while the tropopause temperature was estimated at -62 C. An interesting feature noted in the character of the overshooting tops is a displacement between the position of the overshooting top on visible imagery versus the location of the cold top on infrared. In nearly every case the cold top was found to be slightly upwind from the overshooting top.

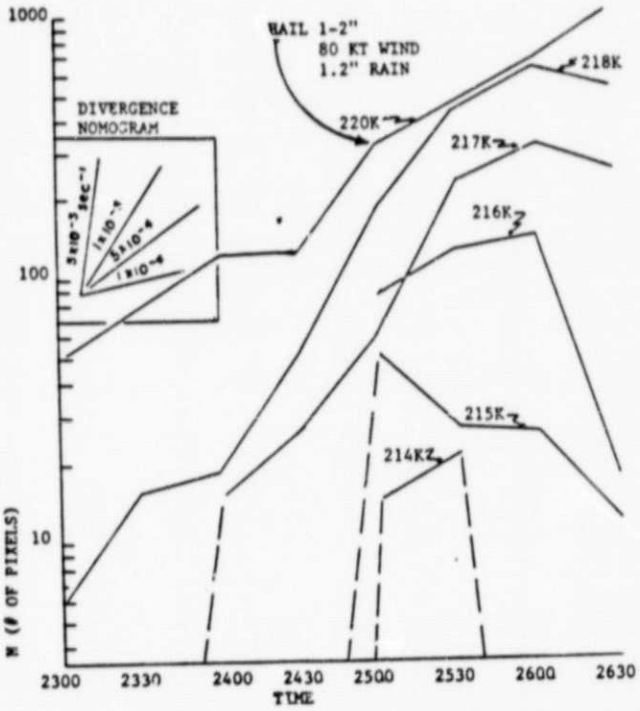

Fig. 29. Temporal variation of the number of pixels enclosed by the given isotherm for temperatures colder than the environmental tropopause for 18 July 1978.

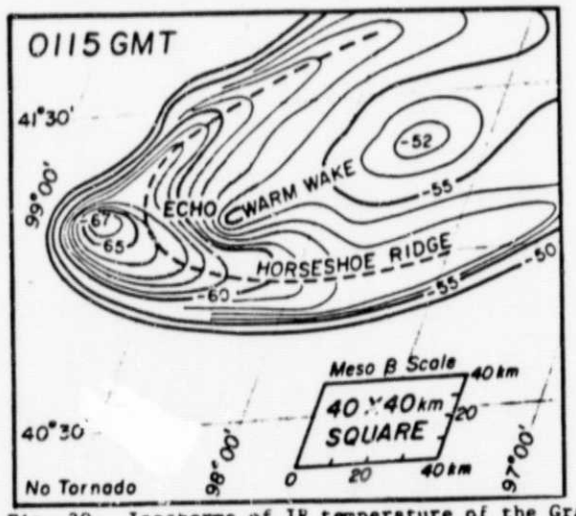

Fig. 30. Isotherms of IR temperature of the Grand Island tornado cloud at 0115 GMT drawn at 1 C intervals. Horseshoe ridges (cold) are shown with dashed arcs and warm depressions, with letters "wake" on the downwind side of radar echoes.

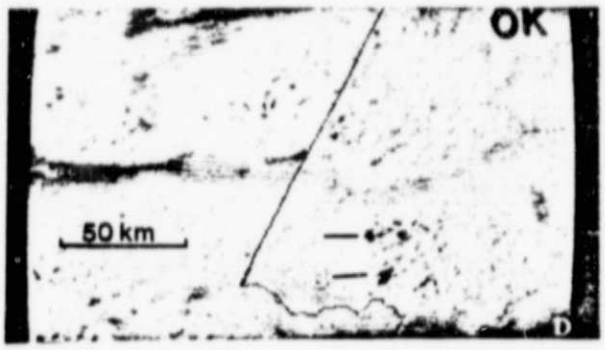

Fig. 31. GOES-East 1 km visible image, 11 May 1982 at 2223 GMT. Note overshooting tops at A and B.

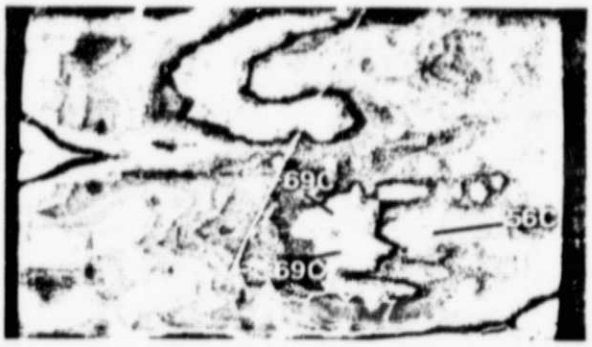

Fig. 32. Same time and area as Fig. 31, but with improved infrared image, note cold "V" and warm wake.

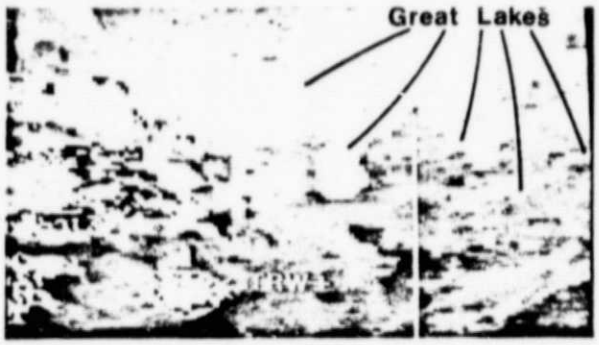

Fig. 34a. 3.9 m channel image for 22 July 1981 at 1702 GMT.

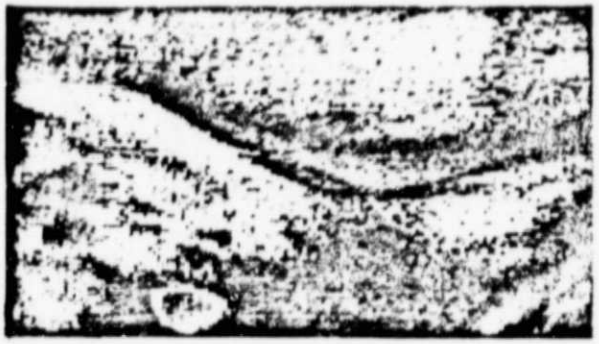

Fig. 34b. 6.7 m channel image, ref. Fig. 34a.

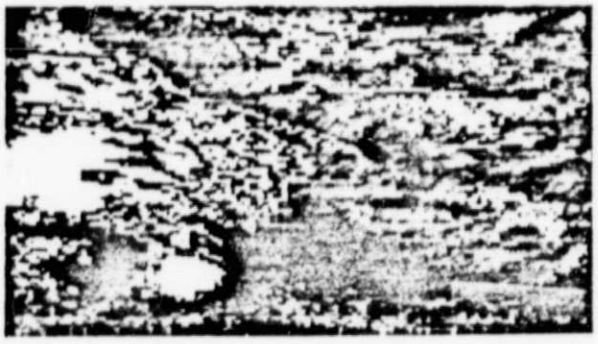

Fig. 34c. 13.3 m channel image, ref. Fig. 34a.

Fig. 34d. 14.0 m channel image, ref. Fig. 34a.

Fig. 34e. 14.2 m channel imge, ref. Fig. 34a.

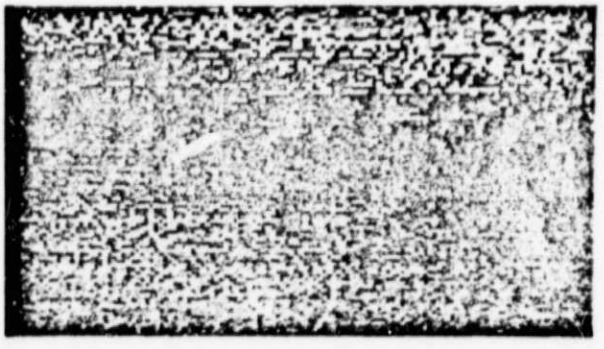

Fig. 34f. 14.5 m channel image, ref. Fig. 34a.

The overshooting top region associated with storm A had been evident on satellite imagery even before the storm moved into Oklahoma. The top from storm B appeared at 2214 GMT and immediately began moving northward while the other top moved northeast. The two tops merged at roughly 2235 GMT, approximately 30 minutes after the lower portions of the two were observed to merge by radar. Satellite data showed an updraft intensification (i.e., a 2 C decrease in cold top temperature) following the storm top merger. This temporary intensification would have increased the pre-existing vorticity associated with the updraft through stretching. It was shortly after the overshooting top merger that tornadic activity began from these storms. Downwind from storm tops A and B is a well defined warming with a cold "V" surrounding the warm wake. Such a signature is also evident with the storm in the upper part of the picture (in the east Central Texas panhandle): that storm also produced tornadic activity. While the "V" notch signature is a good positive indicator of severe storm activity it is not always present when tornadic storms are in being - such was the case for much of the early tornadic storm activity for the March 28, 1984 outbreak previously discussed.

10. SATELLITE SOUNDING INFORMATION FOR MESOSCALE CONVECTIVE APPLICATIONS

Sounding information from GOES/VAS can detect small and significant temporal variations in atmospheric temperature and moisture (Smith, et al, 1981). The sounder on GOES/VAS has seven CO channels, three water vapor channels and two window channels; instrument characteristics that relate to vertical resolution are shown in Table 2 from Zehr and Green (1984).

GOES/VAS can be operated in one of three modes: 1) a normal VISSR mode as with GOES; b) a dwell sounding mode which uses all or most of the sounder channels; and c) a multispectral imaging mode in which VISSR data plus one or two additional VAS channels are sampled. It should be realized that the three possible modes of operation are not independent; when the satellite is operated in one mode data from the other modes are not available. Data from the various VAS channels may be viewed individually or combined to produce mesoscale soundings. Both have applicability for mesoscale convective applications.

10.1. Mesoscale moisture information

The moisture structure of the atmosphere, both in the horizontal and vertical, has long been known to be an important factor in storm development (Doswell & Lemon, 1979): significant variance exists within the mesoscale range below 100 to 200 km. Using sounding information from polar orbiting satellites, Hillger and Vonder Haar (1979, 1981) were able to extract moisture information at a much finer resolution than was available using conventional data sources. Although GOES-VAS is still in the evaluation phase (the system will become operational in mid-1986) similar results concerning mesoscale moisture distribution have been demonstrated (Smith, et al, 1981; Petersen and Mostek, 1982).

There are three water vapor channels on GOES-VAS, table 2. The energy received in each of those channels is a function of the amount of water vapor, its distribution and temperature within a portion of a column in the atmosphere, as well as surface effects (except 6.7 m) and cloud effects. Except where there is significant low level water vapor, the information in the 12.7 m band is similar to the 11.2 m window. Because of that, an interesting product may be derived from the difference in energy between those two bands (12.7 m and 11.2 m). The product, termed "split window" is designed to depict low level water vapor. According to Chesters, et al (1982)

Table 2. VAS Instrument Characteristics

VAS Instrument Characteristics					
			Weighting Function		
Spectral Channel	Central Wavelength (μm)	Absorbing Constituent	Peak Level (mb)	Representative Thickness (mb)	Surface or Cloud Emission Effect
1	14.7	CO_2	40	150-10	usually none
2	14.5	CO_2	70	200-30	nothing below 500mb
3	14.2	CO_2	300	500-10	nothing below 800mb
4	14.0	CO_2	450	800-300	weak
5	13.3	CO_2	950	SFC-500	moderate
6	4.5	CO_2	850	SFC-500	moderate
7	12.7	H_2O	surface	SFC-700	strong
8	11.2	window	surface	----	strong
9	7.2	H_2O	600	800-400	weak at sfc
10	6.7	H_2O	450	700-250	nothing at sfc
11	4.4	CO_2	500	800-100	weak
12	3.9	window	surface	----	strong

The VAS split window clearly differentiates those areas in which water vapor extends over a deep layer and is more able to support convective cells from those areas in which the water vapor is confined to a shallow layer and is therefore less able to support convection.

This type product is very useful over land during the afternoon when there will be a large difference in the signal between the split window channels. However, in the evening when the land temperature has cooled (or over the ocean) the signal differential is small and a meaningful product is difficult to derive.

The 6.7 m channel data (Figure 34b) depict regions of middle level moisture and clouds. Distinct patterns of more moist and cooler areas (blues) and warmer and drier areas (purples) are readily detected. These features are related to areas of both synoptic and mesoscale advection and vertical motion. When viewed in time lapse, they exhibit excellent spatial and temporal continuity. Strong baroclinic regions such as jet streams and vorticity maxima can often be easily identified in cloud free regions by the sharp moisture gradient detected in the 6.7 m image (Anderson, et al, 1982).

Are there clues in the 6.7 m data concerning a storms ability to produce severe weather? Figure 33 is a 6.7 m water vapor image for the storm system of 28 March 1984 previously addressed. Notice the dark region to the south of the storm system - the mid-level air in that region is very dry. As was shown previously, storm relative flow for this case is from the SSE at mid-levels. This points to the likelihood of significant mid-level dry intrusion into the storm system. Such an intrusion of dry air could help fuel the storm's downdraft (outflow) and increase the possibility of that storm producing tornado activity - a sort of forced dynamic/thermodynamic instability. It is interesting to note that the characteristic "V" notch at the thunderstorm top is detectable in the 6.7 m image.

10.2. Thermal channel imagery

The seven VAS thermal channels detect energy proportional to the mean temperature of a layer in the atmosphere if no clouds are present (refer to Table 2). Depending on cloud type, information for certain of the channels may be contaminated (Smith, et al, 1981). Do these channels contain information concerning atmospheric structure? That the answer is "yes" may be verified by examining Figures 34c-f. The area covered by those channels is shown in Figure 34a, from the 3.9 m channel. Figures 34c-f are from channels which receive their energy from progressively higher levels in the atmosphere. In those images, mean layer temperature get progressively colder as one goes from yellow to red to blue. Notice the cloud contamination in all but the highest (stratospheric) channel, and the reflection of surface thermal characteristics (from Figure 34a) in the information in channel 5 (950 mb), figure 34c. The other three channels represent the mean temperature in the troposphere (34d), centered near the tropopause (34e), and in the stratosphere (34f). Note the reversal in the temperature gradient shown in the VAS imagery as one moves from the troposphere to the stratosphere.

Work is currently underway which combines various channels of VAS data in image format to try and detect the development mesoscale structure in the atmosphere. In that work features such as vorticity maxima, jet streaks, thunderstorm complexes, etc. are studied in time lapse in a "system" relative mode similar to that discussed previously. Results look very promising for detecting developing baroclinic regions as well as isolating mesoscale regions of stronger vertical forcing. Such information will certainly aid in helping to solve a variety of mesoscale forecast problems.

10.3. Retrievals from VAS

Initial research with GOES-VAS data concentrated on deriving vertical profiles of temperature and moisture based on observed radiances. Details of the retrieval algorithms are given by Smith (1983). Since that initial research, significant results have been achieved in deriving objective mesoscale convective forecast parameters from VAS retrieval information (Smith, et al, 1984). VAS derived products that are being provided in real-time to the National Severe Storm Forecast Center in Kansas City include: 1) upper and lower level wind analyses derived from VAS thermal field gradient winds and cloud drift winds; 2) analyses of lifted index; 3) 850 mb and 500 mb temperature fields; 4) total precipital water; 5) a thermodynamic stability index similar to a total totals index; and 6) a statistical probability estimate of severe weather presented at 80 km resolution, products 4 and 5 are presented at the full 7 km GOES/VAS resolution as image products.

While combined products from VAS are showing applicability for helping to diagnose the convective storm environment questions still must be answered concerning the utility of individual VAS soundings for such analyses. Figure 35 is a GOES image over the central USA in June of 1984: the numbers within the image give the location of selected VAS soundings for the time period just prior to the time of the image. Notice that sounding 23 is representative of an airmass modified by thunderstorm outflow (it is within the cold dome) while sounding 32 is in air that has not experienced thunderstorm activity. VAS soundings at those two locations are presented in figure 36. Notice that although the VAS information is presented for rather thick layers, the general characteristics one should expect are evident - that is a cooler and more stable low level airmass at location 23 versus that at location 32. VAS sounding 63 is within the cooler air benind a slow moving cold front that is pushing westward across Kansas while VAS sounding 59 is in the more unstable air to its west. These soundings are presented in figure 37: again the results appear as one should expect. Soundings similar to those presented here may be taken by VAS at hourly intervals over cloud free areas of interest. Those soundings contain information on the atmosphere's thermal and moisture characteristics at a spatial and temporal resolution never before available. The question that currently lies before us is "how do we best utilize this information?"

Clouds have historically been viewed as a source of contamination to satellite sounding data. However, work is now underway to try and add information in the cloudy regions. In one

approach information on the atmosphere's thermal and moisture structure is being fine tuned according to the cloud type and structure revealed in GOES visible and infrared imagery. In a similar approach (Smith, et al, 1984) cloud drift winds from the "cloud contaminated regions" are being blended with the thermal information from VAS to improve regional scale analyses.

Fig. 35. GOES-West 1 km visible image, 21 June 1984 at 2315 GMT. Numbers indicate locations of VAS soundings.

11. CONCLUSIONS

The information presented in this chapter has shown how certain characteristics of the atmosphere can be deduced from GOES-VAS sounding and image data. The geostationary satellite has the unique ability to frequently observe the atmosphere (sounders) and its cloud cover (visible and infrared) from the synoptic scale down to the cloud scale. This ability to provide frequent, uniformly calibrated data sets over a broad range of meteorological scales places the geostationary satellite at the very heart of the understanding of mesoscale weather development. By combining satellite data with conventional data, many of the features important in mesoscale weather development and evolution may be better analyzed and understood.

It is through this improved analysis and understanding that mesoscale forecasting will become a reality.

12. ACKNOWLEDGEMENTS

Portions of this work were supported by NASA Grant NAGW - 504 and NOAA Grants NA84AA-H-00020 and NA84AA-D-00017. The author wishes to thank Sallie Varner for preparation of the manuscript.

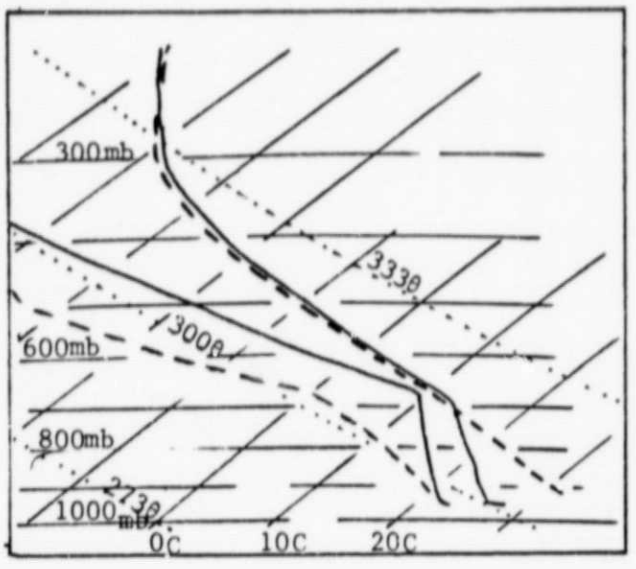

Fig. 36. VAS soundings at locations 23 (T and T_d solid lines) and 32 (T and T_d dashed lines) in Fig. 35.

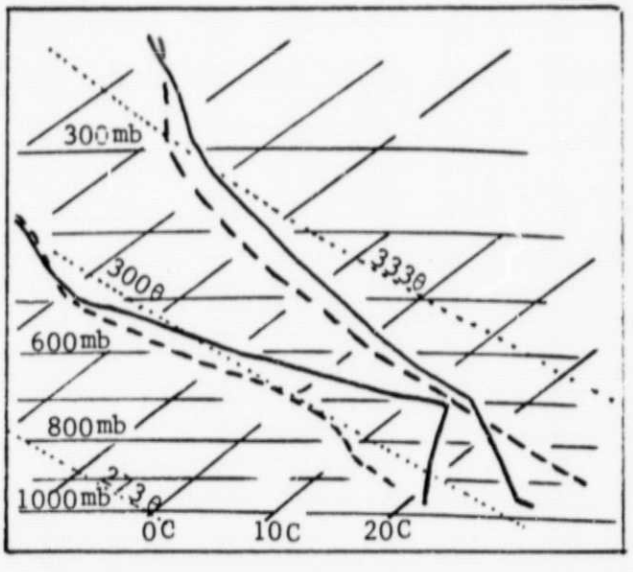

Fig. 37. VAS soundings at locations 59 (T and T_d dashed lines) and 63 (T and T_d solid lines) in Fig. 35.

13. REFERENCES

Achtemeier, G.L., 1983: The relationship between the surface wind field and convective precipitation over the St. Louis area. J. Clim. and Appl. Meteorol., 22, 982-999.

Adler, R.F., and D.D. Fenn, 1977: Satellite based thunderstorm intensity parameters. Preprints 10th Conf. on Severe Local Storms, Omaha, Amer. Meteor. Soc., 8-15.

Adler, R.F., and D.D. Fenn, 1979: Thunderstorm intensity as determined from satellite data. J. Appl. Meteor., 18, 502-517.

Anderson, R.K., J.J. Gurka, and S.J. Steinmetz, 1982: Application of VAS multispectral imagery to aviation forecasting. Preprints 9th Conf. on Weather Forecasting and Analysis, Seattle, Amer. Meteor. Soc., 227-234.

Beebe, R.G. and F.C. Bates, 1955: A mechanism for assisting in the release of convective instability. M.W.R., 83, 1-10.

Bleckman, J.B., 1981: Vortex generation in a numerical thunderstorm model. Mon. Wea. Rev., 109, 1061-1071.

Bohan, W.A., 1981: The importance of thunderstorm outflow boundaries in the development of deep convection. WAB 456, 16mm Color Sound Movie, The Walter A. Bohan Co., 2026 Oakton Street, Park Ridge, IL, 29 minutes.

Brandes, E.A. 1978: Mesocyclone evolution and tornadogenesis: Some observations. Mon. Wea. Rev. 106, 995-1101.

Browning, K.A., 1964: Airflow and precipitation trajectories within severe local storms which travel to the right of the winds. J. Atmos. Sci., 21, 634-639.

Browning, K.A., 1982: Nowcasting, Academic Press Inc., London, New York (U.S. edition), 256 pp.

Byers, H.R., and R. Braham, 1949: The thunderstorm. Govt. Printing Office, Washington, DC, 287 pp.

Caracena, F., R.A. Maddox, J.F.W. Purdom, J.F. Weaver, and R.N. Green, 1983: Multi-scale analyses of meteorological conditions affecting Pan American World Airways Flight 759. NOAA/ERL, Boulder, CO and NOAA/NESDIS, Ft. Collins, CO, 53 pp.

Changnon, S.A., 1976: Effects of urban areas and echo merging on radar echo behavior. J. Appl. Meteor., 15, 561-570.

Chesters, D., L.W. Uccellini and A. Mostek, 1982: VISSR Atmospheric Sounder (VAS) simulation Experiment for a severe storm environment. Mon. Wea. Rev., 110, 198-216.

Darkow, G.L., 1968: The total energy environment of severe storms. J. Appl. Meteor., 7, 199-205.

Doswell, C.A., III, and L.R. Lemon, 1979: An operational evaluation of certain kinematic and thermodynamic parameters associated with severe thunderstorm environments. Preprints 11th Conf. Severe Local Storms, Kansas City, Amer. Meteor. Soc., 397-402.

Droegemier, K., and R.B. Wilhelmson, 1983: Three dimensional numerical simulation of the interaction between a shallow cumulus field and thunderstorm outflow boundary. Preprints 13th Conference on Severe Local Storms, Tulsa, Amer. Meteor. Soc., 245-248.

Espy, J.P., 1841: The Philosophy of Storms. Charles C. Little & James Brown Co., 347 pp.

Estoque, M.A., 1962: The sea breeze as a function of the prevailing synoptic situation. J. Atmos. Sci., 19, 244-250.

Fankhauser, J., 1971: Thunderstorm-environment determined from aircraft and radar observations. Mon. Wea. Rev., 99, 171-192.

Fankhauser, J., 1976: Structure of an evolving hail storm, part II: Thermodynamic structure and airflow in the near environment. Mon. Wea. Rev., 104, 576-587.

Foltz, G.S. and W.M. Gray, 1979: Diurnal variation in the troposphere's energy balance. J. Atmos. Sci., 36, 1450-1466.

Fujita, T.T., 1955: Results of detailed synoptic studies of squall lines. Tellus, 7, 405-436.

Fujita, T.T., 1959: Precipitation and cold air production in mesoscale thunderstorm systems. J. Meteorol., 16, 454-466.

Fujita, T.T., 1978: Manual of downburst identification for Project NIMROD, SMRP Research Paper No. 156, Univ. of Chicago, 103 pp.

Fujita, T.T., 1981: Mesoscale aspects of convective storms. Proceedings IAMAP Symposium: Nowcasting: Mesoscale Observations and Short-Range Prediction, Hamburg, European Space Agency, 3-10.

Fujita, T.T., 1982: Infrared, stereo-height, cloud-motion, and radar-echo analysis of SESAME-day thunderstorms. Proceedings 12th Conf. on Severe Local Storms, San Antonio, Amer. Meteor. Soc., 213-216.

Fujita, T.T. and H.A. Brown, 1958: A study of mesosystems and their radar echos. Bull. Am. Meteorol. Soc., 39, 538-554.

Fujita, T.T., G.S. Forbes, and T.A. Umenhofer, 1976: Close-up view of 20 March 1975 tornadoes: Sinking cloud tops to suction Vortices. Weatherwise, 29(3), 115-132.

Gray, W.M., 1973: Cumulus convection and larger scale circulations I. Broadscale and mesoscale considerations. Mon. Wea. Rev., 101, 839-855.

Green, R.N., and H.A. Parker, 1983: Application of satellite and radar data to severe thunderstorm analysis. Preprints 13th Conference on Severe Local Storms, Tulsa, Amer. Meteor. Soc., 190-193.

Hasler, A.F., 1981: Stereographic observations from geosynchronous satellites: An important new tool for the atmospheric sciences. Bull. Amer. Meteor. Soc., 62, 194-212.

Haurwitz, B., 1947: Comments on the sea breeze circulation. J. Meteor., 4, 1-8.

Hillger, D.W., and T.H. Vonder Haar, 1979: Analysis of satellite infrared soundings of the mesoscale using statistical structure and correlation functions. J. Atmos. Sci., 36, 287-305.

Hillger, D.W., and T.H. Vonder Haar, 1981: Retrieval and use of high-resolution moisture and stability fields from Nimbus 6 HIRS radiances in pre-convective situations. Mon. Wea. Rev., 109, 1788-1806.

Holle, R.L. and M. Maier, 1980: Tornado formation from downdraft interaction in the FACE mesonetwork. Mon. Wea. Rev., 108, 1010-1028.

Humphreys, W.J., 1914: The thunderstorm and its phenomena. Mon. Wea. Rev., 42, 348-380.

Kellog, W.W., 1982: Early satellite program developments. The Conception, Growth, Accomplishments and Future of Meteorological Satellites. NASA Conf. Pub. 2257, NASA, Scientific and Technical Information Branch, Washington, DC, 101 pp.

Klemp, J.B., and R. Rotunno, 1983: A study of the tornadic region within a supercell thunderstorm. J. Atmos. Sci., 40, 359-377.

Klemp, J.B., and R.B. Wilhelmson, 1978: The simulation of three-dimensional convective storm dynamics. J. Atmos. Sci., 35, 1070-1096.

Lilly, D.K. (ed.), 1977: Project SESAME: Planning documentation volume. NOAA/ERL, U.S. Department of Commerce, Boulder, CO, 308 pp.

Lyons, W.A., 1966: Some effects of Lake Michigan upon squall lines and summertime convection. SMRP Res. Pap. 57, Dept. Geophys. Sci., The University of Chicago, 22 pp.

Maddox, R.A., 1976: An evaluation of tornado proximity wind and stability data. Mon. Wea. Rev., 104, 133-142.

Maddox, R.A., 1980: Mesoscale convective complexes. Bull. Am. Met. Soc., 61, 1374-1387.

McCann, D.W., 1981: The enhanced-V, a satellite observable severe storm signature. NOAA Technical Memo, NWS NSSFC-4, 31 pp.

McNider, R.T., G. Jedlovec adn G. Wilson, 1984: Data analysis and model evaluation of the initiation of convection on 24 April 1982, Tenth Conf. on Weather Forecasting and Analysis, Tampa, Amer. Meteor. Soc.

Miller, R.C., 1972: Notes on analysis and severe-storm forecasting procedures of the Air Force Global Weather Central. AWS Technical Report 200 (rev), Air Weather Service (MAC), U.S. Air Force, 190 pp.

Negri, A., and R. Adler, 1981: Relation of satellite-based thunderstorm intensity to radar-estimated rainfall. J. Appl. Meteor., 20, 60-78.

Newton, C.W., 1963: Dynamics of severe convective storms. Meteor. Monogr., 5, No. 27, 33-58.

Parker, W.T., and R.D. Hickey, 1980: The Cheyenne tornado of 16 July 1979. Nat. Wea. Digest, 5, 45-62.

Pearl, E.W., 1974: Characteristics of anvil-top associated with the Poplar Bluff tornado of May 7, 1973. SMRP Res. Paper 119, Univ. of Chicago, 12 pp.

Petersen, R.A., and A. Mostek, 1982: The use of VAS moisture channels in delineating regions of potential convective instability. Preprints 12th Conf. Severe Local Storms, San Antonio, Amer. Meteor. Soc., 168-171.

Pielke, R., 1973: A three-dimensional numerical model of the sea breezes over south Florida. NOAA Tech. Memo. ERL WMPO-2, 136 pp.

Pielke, R., 1974: A three-dimensional numerical model of the sea breezes over south Florida. Mon. Wea. Rev., 102, 115-139.

Pryor, S.P., 1978: Measurement of thunderstorm cloud-top parameters using high-frequency satellite imagery. M.S. Thesis, Dept. of Atmospheric Science, Colorado State University, Fort Collins, CO, 101 pp.

Purdom, J.F.W., 1971: Satellite imagery and severe weather warnings. Preprints, 7th Conf. Severe Local Storms, Kansas City, Amer. Meteor. Soc., 120-127.

Purdom, J.F.W., 1973: Meso-highs and satellite imagery. Mon. Wea. Rev., 101, 180-181.

Purdom, J.F.W., 1976: Some uses of high-resolution GOES imagery in the mesoscale forecasting of convection and its behavior. Mon. Wea. Rev., 104, 1474-1483.

Purdom, J.F.W., 1979: The development and evolution of deep convection. Preprints, 11th Conf. Severe Local Storms, Kansas City, Amer. Meteor. Soc., 143-150.

Purdom, J.F.W., 1983: Diagnosing the the mesoscale state of the atmosphere using satellite data. Preprints, 13th Conf. on Severe Local Storms, Tulsa, Amer. Meteor. Soc., 167-170.

Purdom, J.F.W., 1984: Use of satellite soundings and imagery for nowcasting and very-short-range forecasting. Preprints, Nowcasting II Symposium, Norrkoping, Sweden, European Space Agency, 99-111.

Purdom, J.F.W., and Gurka, J.G., 1974: The effect of early morning cloud cover on afternoon thunderstorm development. Preprints 5th Conf. on Weather Forecasting and Analysis, St. Louis, Amer. Meteor. Soc., 58-60.

Purdom, J.F.W. and K. Marcus, 1982: Thunderstorm trigger mechanisms over the southeast United States. Preprints 12th Conf. Severe Local Storms, San Antonio, Amer. Meteor. Soc., 487-488.

Purdom, J.F.W., and J.F. Weaver, 1982: Nowcasting during the 10 April 1979 tornado outbreak: A satellite perspective. Preprints 12th Conf. Severe Local Storms, San Antonio, Amer. Meteor. Soc., 467-470.

Purdom, J.F.W., and T.H. Vonder Haar, 1983: Product user's guide, enhancing GOES infrared imagery for nowcast applications. Cooperative Institute for Research in the Atmosphere, Colorado State University, Ft. Collins, CO, 21 pp.

Purdom, J.F.W., K.N. Green and H.A. Parker, 1982: Integration of satellite and radar data for short range forecasting and storm diagnostic studies. Preprints 9th Conf. Weather Forecasting and Analysis, Seattle, Amer. Meteor. Soc., 51-55.

Purdom, J.F.W., T.H. Vonder Haar, J.K. Stewart and N.E. Leary, 1984: Diagnosing the severe thunderstorm environment by mesoscale cloud tracking - a new approach and new information. Preprints, Conf. on Satellite Imagery/Remote Sensing and Applications, Clearwater, Amer. Meteor. Soc.. 100-105.

Reynolds, D., 1979: Observations and detection of damaging hailstorms from geosynchronous satellite digital data. Preprints, 11th Conf. Severe Local Storms, Kansas City, Amer. Meteor. Soc., 181-188.

Reynolds, D.A., and E. Smith, 1979: Detailed analysis of composited digital radar and satellite data. Bull. Amer. Meteor. Soc., 60, 1024-1037.

Schereschewsky, P., 1945: Clouds and states of the sky. Handbook of Meteorology, (ed. by Berry, Bollay and Beers), McGraw-Hill, New York, 1068 pp.

Sikdar, D.N., V.E. Suomi, and C.E. Anderson, 1970: Convective transport of mass and energy in severe storms over the United States--An estimate from geostationary altitude. Tellus, 22, 521-532.

Simpson, J.S. and Dennis, A.S., 1974: " Cumulus clouds and their modification." Weather Modification, (W.N. Hess, ed.), Wiley, New York, 229-280.

Sinclair, P.C., and J.F.W. Purdom, 1982: Integration of research aircraft data and 3 minute interval GOES data to study the genesis and development of deep convective storms. Preprints 12th Conf. Severe Local Storms, San Antonio, Amer. Meteor. Soc., 269-271.

Sinclair, P.C., and J.F.W. Purdom, 1984: Aircraft penetrations of arc cloud lines. Preprints Satellite Meteorology/Remote Sensing and Applications, Clearwater, Amer. Meteor. Soc., 160-163.

Smith, W.L., 1983: The retrieval of atmospheric profiles from VAS geostationary radiance observations. J. Atmos. Sci., 40, 2025-2035.

Smith, W.L., V.E. Soumi, W.P. Menzel, H.M. Woolf, L.A. Stromousky, H.E. Revercomb, C.M. Hayden, D.N. Erickson and F.K. Mosher, 1981: First sounding results from VAS-D. Bull. Amer. Meteor. Soc., 62, 232-236.

Smith, W.L., G.S. Wade, W.P. Menzel, V.E. Soumi, K.J. Fox, C.S. Velden, and J.S. Leharshall, 1984: Nowcasting - advances with McIDAS III. Preprints Nowcasting II Symposium, Norrkoping, Sweden, European Space Agency, 433-438.

Weaver, J.F. and J.F.W. Purdom, 1983: Some unusual aspects of thunderstorm cloud top behavior on May 11, 1982. Preprints 13th Conf. on Severe Local Storms, Tulsa, Amer. Meteor. Soc., 154-157.

Wilson, J. and R. Carbone, 1984: Nowcasting with Doppler radar: forecaster-computer relationship. Preprints, Nowcasting II Symposium, Norrkoping, Sweden, European Space Agency, 177-186.

Zehr, R.M., 1982: Thunderstorm motion analyses. Preprints 9th Conference on Weather Forecasting and Analysis, Seattle, Amer. Meteor. Soc., 455-458.

Zehr, R.M., and K.N. Green, 1984: Mesoscale applications of VAS imagery. Preprints Conf. on Satellite Meteorology/Remote Sensing and Appl., Clearwater Beach, Amer. Meteor. Soc., 94-98.

Zipser, E.J., 1984: The National STORM program, STORM central phase preliminary program design. National Center for Atmsopheric Research, Boulder, CO, 147 pp.